

Variability in optical particle backscattering in contrasting bio-optical oceanic regimes

David Antoine,^{a,*} David A. Siegel,^{b,c} Tihomir Kostadinov,^b Stéphane Maritorena,^b Norm B. Nelson,^b Bernard Gentili,^a Vincenzo Vellucci,^a and Nathalie Guillocheau^b

^aLaboratoire d’Océanographie de Villefranche, Centre National de la Recherche Scientifique and Université Pierre et Marie Curie, Paris 06, CNRS, Villefranche-sur-Mer, France

^bEarth Research Institute, University of California at Santa Barbara, Santa Barbara, California

^cDepartment of Geography, University of California at Santa Barbara, Santa Barbara, California

Abstract

Variability in the optical particle backscattering coefficient (b_{bp}) is investigated in oceanic waters from two sites, namely the BOUée pour l’acquiSition d’une Série Optique à Long termE site in the northwestern Mediterranean Sea and the Plumes and Blooms stations in the Santa Barbara Channel off Southern California. Data from these two sites span two orders of magnitude in b_{bp} and likely cover typical open ocean values. A significant relationship is found between b_{bp} at wavelengths of 442 and 555 nm and chlorophyll concentration. However the large spread in this relationship makes chlorophyll a poor predictor of b_{bp} . The relationship between b_{bp} and the particulate beam attenuation coefficient at 660 nm is tighter for both sites, indicating covariability of the particle size ranges that determine both coefficients. A detailed study of the seasonal changes of the b_{bp} vs. chlorophyll relationship reveals that this bio-optical relationship might be best described as a succession of distinct regimes with rapid transitions from one to another. The backscattering ratio (\tilde{b}_{bp} ; the ratio of b_{bp} to total particulate scattering, b_p) ranges from about 0.2% to 1.5%, which is similar to previously reported values. The relationship between \tilde{b}_{bp} and chlorophyll was not significant, while values of the backscattering ratio varied spectrally.

Optical backscattering refers to the scattering of visible electromagnetic radiation in the backward direction with respect to the direction of propagation. The backscattering coefficient, b_b (m^{-1} ; see Table 1 for symbol definitions and units), is an inherent optical property (IOP; Preisendorfer 1961) and a function of the volume scattering function (VSF), $\beta(\lambda, \theta)$ (VSF with units m^{-1} steradian⁻¹ [sr^{-1}], where θ is the scattering angle [$\theta = 0$ for the direction of propagation] and λ the wavelength), through

$$b_b(\lambda) = 2\pi \int_{\pi/2}^{\pi} \beta(\lambda, \theta) \sin(\theta) d\theta \quad (1)$$

Seawater, inorganic and organic living or nonliving particles, and bubbles all additively contribute to b_b . Determining how the relative contributions of these components vary as a function of the physical and bio-optical state of oceanic waters remains an elusive task (Stramski et al. 2004). This work focuses on the role of particles with regard to optical backscattering. In the following, coefficients pertaining to pure seawater will be identified by the ‘w’ subscript, whereas ‘p’ will indiscriminately indicate particles, and ‘ φ ’ will specifically refer to phytoplankton. Hence, backscattering by particles, b_{bp} , can be described as follows:

$$b_{bp}(\lambda) = b_b(\lambda) - b_{bw}(\lambda) \quad (2)$$

The scattering coefficient of pure seawater (b_w , with $b_{bw} = b_w/2$) has been reassessed by Zhang et al. (2009) and Zhang

and Hu (2009). Their parameterization includes the effects of temperature and salinity. It is used here and provides very close results compared to the work of Twardowski et al. (2007). The shape and magnitude of the particle VSF for angles $> 90^\circ$ —hence, the magnitude of b_{bp} —are determined by the concentration of particles, their index of refraction (composition), their shape, and by the particle size distribution (PSD) over the size range that matters for the wavelengths under consideration. To remove the first-order effects of particle concentration, the particle backscattering ratio (or backscattering probability) is defined as

$$\tilde{b}_{bp}(\lambda) = b_{bp}(\lambda)/b_p(\lambda) \quad (3)$$

where b_p is the particulate scattering coefficient.

The importance of determining spectral values of b_{bp} in the ocean stems from the tight link to essential physical and chemical characteristics of particles (Boss et al. 2004a,b). Accurate determinations of b_{bp} carry information about the composition of particles (Twardowski et al. 2001; Boss et al. 2004b) and potentially information on the relative contributions of living and nonliving (mineral) particulates. When spectral b_{bp} measurements are available, parameters of a log-linear PSD can be estimated (with some limitations; Kostadinov et al. 2009). Understanding the PSD has tremendous importance because it provides a measure of the structure and functioning of the pelagic ecosystems (Le Quéré et al. 2005; Kostadinov et al. 2010), can be used to constrain particle sinking rates, and can aid in elucidating the ocean’s role in carbon sequestration.

Accurate b_{bp} determinations are also of paramount importance for the interpretation of the remotely sensed signal provided by satellite-borne ocean color sensors

* Corresponding author: antoine@obs-vlfr.fr

(Gordon and Morel 1983). These sensors essentially measure the radiance exiting the ocean, which to first order is proportional to the backscattering coefficient and inversely proportional to the absorption coefficient (a). Correct interpretation of the ocean color signal and closure analyses require accurate determinations of a and b_b .

Unfortunately, knowledge of b_{bp} remains limited in spite of its high level of importance in building optical closure and interpreting ocean color signals. Little is actually known about the intermingled implications of the various parameters that determine b_{bp} (see the review by Stramski et al. [2004]). One difficulty lies in the limited number of in situ measurements of either the full VSF or the backscattering coefficient.

Another reason for this slow progress toward a better understanding of b_b is the inappropriateness of theoretical computations (i.e., computations performed with Mie theory [Mie 1908; van de Hulst 1981]). Although the applicability of Mie theory to the determination of backscattering is known to be limited (Bohren and Singham 1991), it is the only available theory, and, hence, it is often used. Semi-analytical models of backscattering by oceanic particles often adjust their parameterizations in order to have, for instance, spectral changes of b_{bp} that respect Mie theory predictions (Morel and Maritorena 2001). In addition, although the role of phytoplankton is generally considered minor in determining b_{bp} (according to Mie theory; Stramski and Kiefer 1991; Stramski et al. 2004), parameterizations of b_{bp} often derive from observations on pure phytoplankton cultures that have little to do with the real environment in terms of composition of the overall particle pool (Ahn et al. 1992). New evidence indicates that phytoplankton-sized particles may contribute more to backscattering than has been previously thought (Dall'Olmo et al. 2009).

A third difficulty lies in the determination of the particle characteristics, in terms of composition, shape, structure (homogeneous, multi-layers, etc.), and size distribution. Measurement of these properties is extremely difficult, and most of the existing techniques for the determination of the PSD often do not provide measures of the contribution of submicronic particles, which are suspected to dominate particulate backscattering (Morel and Ahn 1991; Stramski and Kiefer 1991).

Therefore, many questions are still unresolved concerning the variability and controls on b_{bp} . It is unclear, for instance, whether b_{bp} is spectrally variable or not or whether a robust relationship exists between b_{bp} and the chlorophyll concentration ($[Chl]$). Large uncertainties remain, in particular about b_{bp} in clear oceanic waters ($[Chl] < \sim 0.2 \text{ mg m}^{-3}$; i.e., about 50% of the ocean area). One way to progressively answer these questions is to analyze more concurrent in situ measurements of b_{bp} and of environmental parameters that regulate its variations (such as $[Chl]$). This is precisely the focus of the present work, through which the following questions are addressed: (1) Is there a ubiquitous relationship between b_{bp} and chlorophyll in Case 1 waters (Morel and Prieur 1977), and does it extend into the low-chlorophyll waters? (2) How do b_{bp} and chlorophyll seasonal cycles compare? Are their

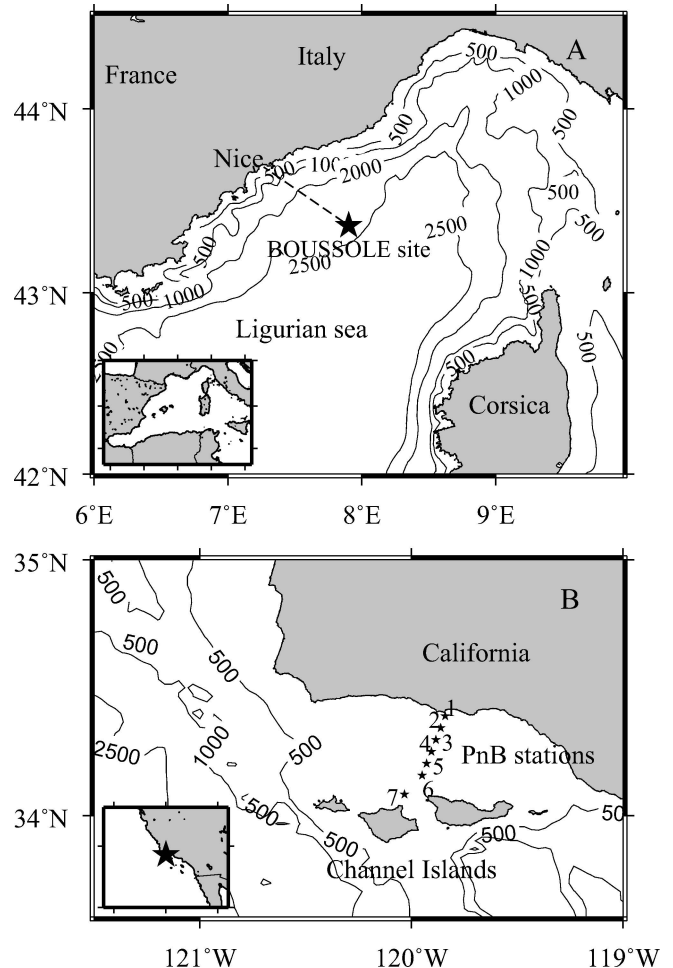


Fig. 1. Maps of the two measurement sites: (A) BOUSSOLE in the northwestern Mediterranean Sea and (B) PnB in the Santa Barbara Channel, California. Station locations are indicated with stars. Bathymetry is in meters.

amplitudes similar? Is there occasionally a significant time lag between both? (3) How does b_{bp} vary with chlorophyll or with wavelength?

Data from two oceanic sites are used here: BOUée pour l'acquiSition d'une Série Optique à Long termE (BOUSSOLE; a French acronym that literally translates as "Buoy for the acquisition of a long-term optical time series"; Antoine et al. 2006; <http://www.obs-vlfr.fr/Boussole>) and Plumes and Blooms (PnB; Toole and Siegel 2001; Otero and Siegel 2004; Kostadinov et al. 2007; <http://www.icess.ucsb.edu/PnB/PnB.html>). Their locations are shown in Fig. 1. The conditions at BOUSSOLE are essentially oligotrophic to mesotrophic, while the PnB stations are coastal. The rationale is to assess variations in b_{bp} measurements collected over a large range of bio-optical states and to address their relationships with ecologically relevant properties.

Methods

Description of field sites—Essential information about the site characteristics (see Fig. 1 for their locations), the

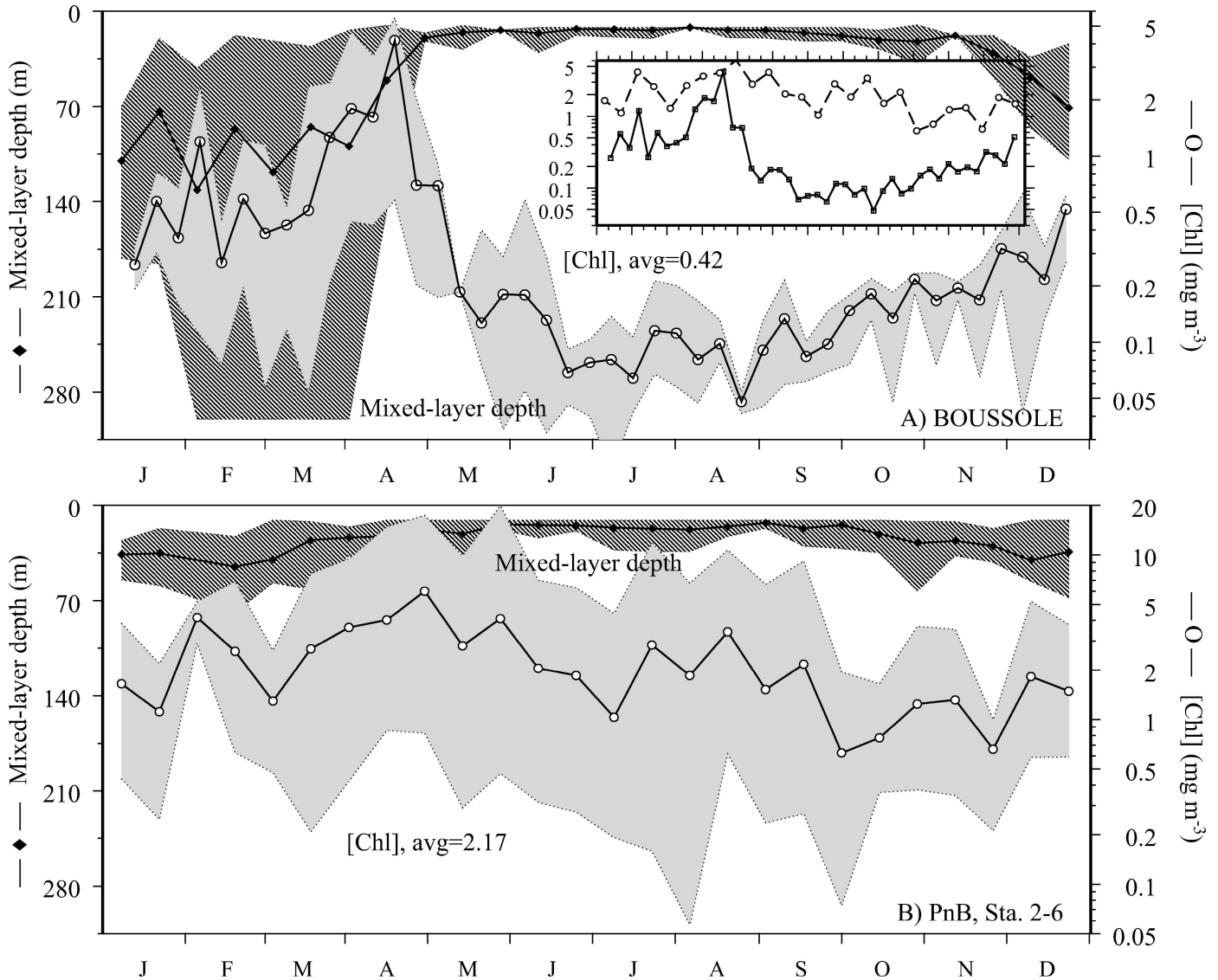


Fig. 2. Average seasonal cycles of the mixed-layer depth (Z_{ml}) and surface ($< 10\text{-m}$) chlorophyll concentration ($[Chl]$) at the two measurement sites (panel A is for the BOUSSOLE site and panel B for PnB stations). Average $[Chl]$ values are indicated, and the shaded areas are the SDs around the average cycles. The average cycles at BOUSSOLE were obtained from 16 yr of $[Chl]$ data (1991–2006) and 11 yr of Z_{ml} data (1994–2004). Both $[Chl]$ and Z_{ml} were averaged over the same 10 yr at PnB (1996–2005; Sta. 2–6 only). The insert in (A) shows the chlorophyll cycles for the two sites with the same scale.

measurement platforms, and the instrumentation is provided in Antoine et al. (2006, 2008b) for BOUSSOLE and in Kostadinov (2005) and Kostadinov et al. (2007) for PnB. Therefore, the observation sites are described only briefly here for the sake of completeness; we include information relevant to the present study. In particular, the typical seasonal cycles of the upper-ocean mixed layer (Z_{ml}) and of the surface ($< 10\text{ m}$) $[Chl]$ at the two sites are displayed in Fig. 2 and discussed below, because these two properties have a determining influence on the seasonal dynamics of particles.

The BOUSSOLE project started in 2000, and its activities are developed on a site located in the northwestern Mediterranean Sea, at about 32 nautical miles from the coast (Fig. 1A). This site is protected from coastal inputs

by the Ligurian Current, which flows along the coast toward the southwest (Millot 1999). An important seasonality exists in the physical conditions in this area (Fig. 2A), with deep mixed layers in winter, usually $\sim 400\text{ m}$ and occasionally down to the bottom at 2440 m, and a marked stratification in summer, with $Z_{ml} \sim 20\text{ m}$. This dynamic drives the seasonal changes in phytoplankton, with oligotrophic conditions prevailing in summer ($[Chl] < \sim 0.1\text{ mg m}^{-3}$, with minima around 0.05 mg m^{-3}), concentrations up to $\sim 3\text{--}5\text{ mg m}^{-3}$ during the spring phytoplankton bloom (February to March or April), and $[Chl]$ of $\sim 0.1\text{--}0.3\text{ mg m}^{-3}$ the rest of the year. This cycle is typical of mid-latitude temperate seas. There is, accordingly, a large range of optical properties at this site (Antoine et al. 2006), as is the case over the entire northwestern

Mediterranean Sea (Morel and André 1991; Bosc et al. 2004).

A buoy has been permanently deployed at the BOUSSOLE site since September 2003 and operates in a quasi-continuous mode, with data acquisition every 15 min night and day. This platform was specifically designed to optimize the measurement of radiometric quantities at two depths in the water column, nominally 4 m and 9 m, and at + 4.5 m above the surface (Antoine et al. 2008b), from which apparent optical properties (AOPs) and inherent optical properties (IOPs) are derived. Two sister buoys equipped with the same sets of instruments are swapped about every 6 months. Adequate measures have to be taken to minimize or eliminate bio-fouling, which is unavoidable with moored instruments. All instruments installed on the BOUSSOLE buoy are cleaned by divers every 2 weeks; in addition, copper tape is used on the instrument housings for transmissometers, copper rings on emission and reception windows of transmissometers, and copper faceplates for the backscattering meters. These practical measures have proven efficient in preventing bio-fouling. Possible contamination that would have developed in spite of these procedures is identified by comparison of the data collected before and after the cleaning operations, which allows elimination of possibly corrupted data. The BOUSSOLE site has been visited monthly since July 2001, during which time 0–400-m casts have been performed for acquisition of hydrological (conductivity–temperature–depth, CTD) data, complementary IOPs and AOPs, and water sampling for subsequent phytoplankton pigment analyses (high-performance liquid chromatography, HPLC) and particulate absorption measurements.

The PnB project began in August 1996 and consists of monthly sampling of physical, biological, chemical, and a comprehensive suite of optical measurements at seven stations spanning the Santa Barbara Channel (SBC; Fig. 1B). The SBC is an optically complex coastal site in which optical properties are affected by phytoplankton blooms, sediment plumes, and other episodic events, including mixing of various water masses (Toole and Siegel 2001; Otero and Siegel 2004; Kostadinov et al. 2007). There is a complex mix of cold water of relatively low salinity upwelled off Point Conception and warm, saltier Southern California Bight waters (Harms and Winant 1998). During the spring and early summer, upwelling introduces nutrient-rich water into the SBC, leading to blooms of phytoplankton. Finally, late-winter storms input sediment-laden waters into the SBC, mainly from the Santa Clara and Ventura Rivers (Otero and Siegel 2004). These intermingled influences lead to the pattern shown in Fig. 2B (the two shallow-water stations, Sta. 1 and Sta. 7, being excluded), with a rather seasonally stable mixed-layer depth (20–50 m) and average [Chl] of around 2 mg m^{-3} , with higher chlorophyll levels from April to July and lower values in the fall. Intense blooms are found within the SBC, usually in late spring (Toole and Siegel 2001; Otero and Siegel 2004). However, the timing of the spring blooms varies enough from year to year to smear out the mean annual cycle signal (Fig. 2B).

Table 1. Symbol definitions.

λ	Wavelength	nm
β	Volume scattering function	$\text{m}^{-1} \text{sr}^{-1}$
[Chl]	Chlorophyll concentration	mg m^{-3}
$a(\lambda)$	Total absorption coefficient	m^{-1}
$a_p(\lambda)$	Particulate absorption coefficient	m^{-1}
$b_b(\lambda)$	Total backscattering coefficient	m^{-1}
$b_{bp}(\lambda)$	Particulate backscattering coefficient	m^{-1}
$b_{bp}(\lambda)$	Particulate backscattering ratio: $b_{bp}(\lambda) : b_p(\lambda)$	Dimensionless
$b_{bw}(\lambda)$	Pure water backscattering coefficient	m^{-1}
$c_p(\lambda)$	Particulate beam attenuation coefficient	m^{-1}
$c_p^*(\lambda)$	Chl-specific attenuation coefficient: $c_p(\lambda) : \text{Chl}$	$\text{m}^2 \text{mg}^{-1}$

Optical backscattering measurements—The volume scattering function at 140° , $\beta(140)$, is measured at BOUSSOLE using HOBILabs® Hydroscat-2 backscattering meters (Maffione and Dana 1997) installed at the lower measurement depth of the buoy ($\sim 9 \text{ m}$) and equipped with filters at 442 and 555 nm (Table 2). Starting in October of 2007, HOBILabs® Hydroscat-4 backscattering meters are used, with bands at 442, 488, 550, and 620 nm. These instruments are factory calibrated before and after each deployment following the method of Maffione and Dana (1997). Dark current measurements, performed on site with a neoprene cap covering the instrument windows, are typically $\sim 1 \times 10^{-5} \text{ m}^{-1} \text{sr}^{-1}$ for $\lambda = 555 \text{ nm}$ and $2 \times 10^{-6} \text{ m}^{-1} \text{sr}^{-1}$ for $\lambda = 442 \text{ nm}$. These numbers represent $\sim 5\%$ of $\beta(140)$ at $\lambda = 555 \text{ nm}$ and $\sim 0.5\%$ at $\lambda = 442 \text{ nm}$. The time series used here is made of measurements from three instruments, starting with one instrument that was used until 09 June 2006 and from 22 February to 21 September 2007, a second one that was used from 10 June 2006 to 21 February 2007, and a third one that has been used since October 2007. Biases between successive deployments were removed to ensure coherency of the time series (only needed for $\lambda = 442 \text{ nm}$), assuming the more reliable measurement is given by the newly calibrated and newly deployed instrument. The instruments operate at 1 Hz, so about 60 measurements are collected during each of the 1-min data collection sequences, conducted every 15 min. The median of these 60 measurements is used to derive a representative value for $\beta(140)$. The median of all these $\beta(140)$ values taken before 07:00 h and after 18:00 h provides the daily values used in this work. Possible diurnal variations are therefore ignored. These median values exclude measurements taken during daylight as a result of their higher noise levels. Although backscattering measurements started in September 2003, these measurements are more systematic after 2005, when the prevention of bio-fouling became more successful. Therefore, only data from 2006 and 2007 are used here.

b_{bp} is derived from $\beta(140)$ as follows (Maffione and Dana 1997; Boss and Pegau 2001):

$$b_{bp} = 2\pi\chi_p(\beta(140) - \beta_w(140)) \quad (4)$$

where $\chi_p = 1.13$ (D. R. Dana and R. A. Maffione unpubl.)

Table 2. Characteristics of the measurement data set. na, not applicable.

Parameter	Site*	Instrument†	Wavelengths (nm)	Measurement depth and frequency
$\beta(\lambda, 140)$	B	Hobilabs® Hydroscat-2 and -4 ¹	442 and 555	1-min measurement sequences at 10 Hz every 15 min, $z=9$ m.
	P	Hobilabs® Hydroscat-6 ²	442, 470, 510, 589, 671, and 870	
$b_p(\lambda)$	B	Wetlabs® AC-9 ³	412, 440, 488, 510, 532, 555, 650, 676, and 715	Profiling mode, during monthly cruises
	P	Wetlabs® AC-9 ⁴	412, 440, 488, 510, 555, 630, 650, 676, and 715	
$c(\lambda)$	B	Wetlabs® 25-cm path length C-star transmissometer ⁵	660	1-min measurement sequences at 6 Hz every 15 min (buoy; $z=4$ and 9 m), plus profiling mode during monthly cruises
	P	Wetlabs® AC-9 ⁴	650	
Phyto-plankton pigments and [Chl]	B	HPLC ⁶	na	Water sampling from a 12-bottle rosette, during monthly cruises
	P	Fluorimetry ⁷		
$a_p(\lambda)$	B	Perkin-Elmer® Lambda 19 ⁸	from 350 to 750, 2-nm resolution	Water sampling from a 12-bottle rosette, during monthly cruises
	P	Shimadzu® UV2401-PC (a Perkin-Elmer® Lambda 2 before mid-2003) spectrophotometer ⁹	from 190 to 900, 0.1-nm resolution 350–750 used in analysis	

* B, BOUSSOLE; P, PnB.

† Superscripted numerals are defined as follows: 1, Maffione and Dana (1997), Antoine et al. (2006); 2, Maffione and Dana (1997), Kostadinov et al. (2007); 3, Antoine et al. (2006); 4, Kostadinov et al. (2007); 5, Antoine et al. (2006); 6, Ras et al. (2008); 7, Kostadinov et al. (2007); 8, Antoine et al. (2006); 9, Kostadinov et al. (2007).

and where $\beta_w(140)$, the contribution of pure seawater to scattering at 140° , is computed following the method of Zhang et al. (2009) using the temperature and salinity measured at the same depth with a Seabird® SBE-37SI CTD sensor. Before entering into Eq. 4, $\beta(140)$ is corrected for attenuation along the measurement path [the $\sigma(\lambda)$ correction of Maffione and Dana 1997] using the beam attenuation coefficient measured in parallel (*see later*) and the total absorption coefficient derived from inversion of the diffuse attenuation coefficient for downward irradiance (K_d) and the irradiance reflectance (R) (eqs. 12 and 13 in Morel et al. 2006). The median value of this correction is $\sim 1.7 \times 10^{-5} \text{ m}^{-1} \text{ sr}^{-1}$ at 555 nm and $5 \times 10^{-5} \text{ m}^{-1} \text{ sr}^{-1}$ at 442 nm. Maximum values of $\sim 5 \times 10^{-4} \text{ m}^{-1} \text{ sr}^{-1}$ occur at $\lambda = 442$ nm when [Chl] $\sim 3\text{--}5 \text{ mg m}^{-3}$. Multiplying the $\beta(140)$ dark current measurements reported above by the $2\pi\chi_p$ factor (Eq. 4) gives uncertainties on total b_b of about $1 \times 10^{-4} \text{ m}^{-1}$ for $\lambda = 555$ nm and $1.5 \times 10^{-5} \text{ m}^{-1}$ for $\lambda = 443$ nm. These numbers are actually smaller than the noise levels provided by the manufacturer (2×10^{-5} to $2 \times 10^{-4} \text{ m}^{-1}$ root mean square error, RMSE). Spectral measurements of the VSF from 0.2° to 178° at a 1° resolution have also been conducted during a single cruise in August of 2004 using the Multispectral Volume Scattering Meter (MVSM) instrument described by Lee and Lewis (2003) and operated as described in Chami et al. (2005). These data were used in complement to the Hydroscat data when analyzing b_{bp} spectral dependence.

A HOBILabs® Hydroscat-6 backscattering meter (Maffione and Dana 1997) is used on PnB cruises in a profiling

mode, with filters at 442, 470, 510, 589, 671, and 870 nm (Table 2). This instrument is pure-water calibrated, either at the factory or at the University of California at Santa Barbara (Kostadinov et al. 2007). The data processing is the same as for the BOUSSOLE measurements, except that the sigma correction is applied using concurrent Wetlabs® absorption and attenuation meter (AC-9) data. Surface backscattering coefficients are determined as the average over the top 15 m. The particle backscattering coefficient at 555 nm is extrapolated from the measurements at 589 nm assuming a λ^{-1} spectral dependency. A large uncertainty of 1 on the exponent would translate only as a 6% uncertainty on $b_{bp}(555)$.

For both data sets, the spectral dependency of b_{bp} is expressed through the slope γ , thus:

$$\gamma = - \frac{\log[b_{bp}(\lambda_1)/b_{bp}(\lambda_2)]}{\log[\lambda_1/\lambda_2]} \quad (5)$$

with $\lambda_1 = 442$ nm and $\lambda_2 = 555$ nm for BOUSSOLE or 589 nm for PnB (i.e., the values extrapolated at 555 nm are not used to compute γ). Under the assumptions that the PSD follows a power law and that the particles are nonabsorbing, γ can be used as a proxy of the slope of the particle size distribution (Morel 1973). The assumption of nonabsorbing particles is invalid, however, and the particulate scattering spectrum is depressed by absorption, in particular at 443 nm (Babin et al. 2003). Loisel et al. (2006) demonstrated the feasibility of retrieving γ from space and related its value to ecosystem characteristics and used it to qualitatively describe

the PSD. Recent investigations relaxed the nonabsorption assumption and theoretically linked γ to the PSD power-law parameters quantitatively, allowing their retrieval from ocean color data (Kostadinov et al. 2009). However, γ is sensitive to the wavelength range from which it is computed and is also sensitive to the measurement noise (McKee et al. 2009). Therefore, the use of γ to investigate dynamics of the PSD is here only qualitative. Low γ values (say, between about 0 and 1) would indicate that large particles dominate, whereas larger values (say, above about 2) would indicate that the community is dominated by smaller particles. Discussing more subtle changes in γ is inappropriate considering the strong limitation of determining its value from two wavelengths only, with one of them being affected by absorption, in particular by phytoplankton (443 nm).

Particulate scattering coefficient—At BOUSSOLE, a WetLabs® AC-9 attenuation and absorption meter (bands at 412, 440, 488, 510, 532, 555, 650, 676, and 715 nm) is deployed on profiling mode during the monthly cruises to the site, providing measurements of $c(\lambda)$ and $a(\lambda)$, from which $b(\lambda)$ is derived by difference (Antoine et al. 2006). A similar instrument is deployed on the PnB cruises, with a slightly different band set (i.e., 412, 440, 488, 510, 555, 630, 650, 676, and 715 nm) (Kostadinov et al. 2007).

Beam attenuation coefficient—The beam attenuation coefficient at 660 nm, $c(660)$, is measured at BOUSSOLE at depths of 4 m and 9 m with 25-cm-path length WETLabs® C-star transmissometers (Table 2; acceptance angle of 1.2°). The particulate beam attenuation coefficient (c_p) is computed as $c - c_w$, with $c_w(660) = 0.364 \text{ m}^{-1}$ (Bishop 1986). This assumes that absorption, by colored dissolved substances organic matter (CDOM) in particular, is negligible at 660 nm (Bricaud et al. 1981). It was also verified that $a_p(660)$ is on average only $\sim 5\%$ of $c_p(660)$ at BOUSSOLE. The same instruments are deployed on the monthly casts, and their measurements are used to correct the buoy transmissometer data for possible drifts. Buoy c_p values are not corrected for a deep background value, as is usually done when using c_p vertical profiles, because correcting for the deep background is incompatible with the buoy b_{bp} measurements, which in essence cover the total pool of particles and cannot be corrected for a deep background value.

At PnB, the surface beam attenuation coefficient is calculated from profile measurements at 650 nm with the AC-9 (averaging the top 15 m of data), and the surface particulate beam attenuation at 650 nm is estimated by subtracting the absorption due to CDOM at 650 nm, as measured by the laboratory spectrophotometer (Table 2) for discrete surface-water samples.

The particle backscattering probability (\tilde{b}_{bp}) is determined using Eq. 3. For BOUSSOLE, b_p is computed in three different ways. The first uses the buoy measurements of the particulate beam attenuation coefficient at 660 nm, $c_p(660)$, and assumes that particulate and CDOM absorption are negligible at 660 nm [so $c_p(660) = b_p(660)$] and that the particle scattering coefficient is spectrally flat [i.e., $b_p(\lambda) = b_p(660)$], which is supported by the BOUSSOLE AC-9

observations (not shown). The second technique uses $b_p(\lambda)$, as determined from chlorophyll using the $b_p(\lambda)$ -to-chlorophyll relationship established from the BOUSSOLE AC-9-derived b_p values. The third solution uses $b_p(\lambda)$ as determined from chlorophyll using existing bio-optical parameterizations. The data from the MVSM instrument are also used here to complement other determinations of the particle backscattering ratio. At PnB, \tilde{b}_{bp} is computed as $b_{bp}(\lambda)/b_p(\lambda)$ using AC-9 determinations for $b_p(\lambda)$, linearly interpolated to the respective Hydroscat-6 wavelengths (Kostadinov et al. 2007).

Phytoplankton pigments and particulate absorption—Water sampling is performed during the BOUSSOLE cruises between the surface and a depth of 200 m, from which only the data obtained from samples at 5 m and 10 m are used here. Particles are collected onto 25-mm Whatman glass-fiber filters GF/F (0.7- μm porosity) and then stored in liquid nitrogen, until algae pigment contents are measured in the laboratory using HPLC, following the method of Ras et al. (2008). The total chlorophyll *a* concentration ([Chl]) is computed as the sum of the concentrations of Chl *a* (including allomers and epimers), chlorophyllide *a* plus divinyl Chl *a*. Before pigments are extracted, the filters are used to determine spectral particulate absorption, $a_p(\lambda)$, with a Perkin-Elmer Lambda 19 dual-path spectrometer with an integrating sphere compartment attached (Antoine et al. 2006). Phytoplankton and nonalgal particle absorption are determined by numerical decomposition following the method of Bricaud and Stramski (1990).

In order to interpret IOP changes at the daily scale (buoy measurements), a reconstructed cycle of daily chlorophyll values is built by combining the HPLC determinations with satellite-derived daily chlorophyll values (Antoine et al. 2008a).

For PnB, data obtained from fluorometric chlorophyll measurements are used here. Particulate and phytoplankton absorption are measured as well. See Table 2 and Kostadinov et al. (2007) for details.

Results

Water types at the two sites—Field determinations of the surface irradiance reflectance at 560 nm, $R(560)$, are displayed as a function of [Chl] in Fig. 3. Also shown is the theoretical upper limit of $R(560)$ for Case 1 waters, $R_{lim}(560)$, following the method of Morel and Bélanger (2006). Data from the two sites are essentially below the theoretical curve, which means that the BOUSSOLE site and the deep-water PnB stations (Sta. 2–6) are all Case 1 waters. Exceptions occur relatively infrequently at low chlorophyll values at BOUSSOLE and at higher chlorophyll values for PnB. This confirms that an appropriate value of $R_{lim}(560)$ remains elusive in the low-chlorophyll domain (Morel and Bélanger 2006).

General characteristics of the two particle backscattering data sets—The 2-yr time series of $b_{bp}(555)$, γ (Eq. 5), and [Chl] at BOUSSOLE are displayed in Fig. 4A, and the ~ 4.5 -yr time series of the same parameters at PnB is

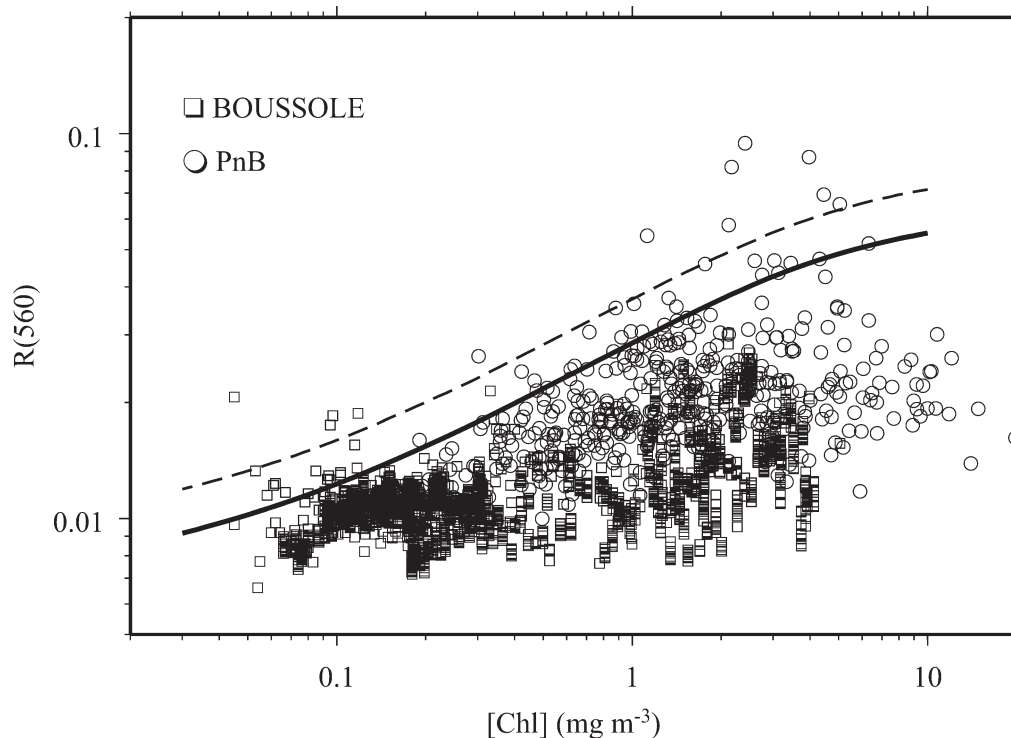


Fig. 3. Irradiance reflectance at 560 nm, $R(560)$, as a function of $[Chl]$. The points for BOUSSOLE are from 3 yr of clear-sky quality-checked buoy measurements taken within 1 h of solar noon. All available measurements from 1996 to 2005 are used at PnB. The solid curve is the theoretical upper limit for Case 1 waters (Morel and Bélanger 2006), $R_{lim}(560)$, and the dashed curve is $R_{lim}(560) \times 1.3$.

displayed in Fig. 4B. For BOUSSOLE, daily average values are shown for $[Chl]$; daily average and monthly average values for $b_{bp}(555)$; and monthly average values for γ . For PnB, all three parameters are shown as average values over each cruise and over the deep-water Sta. 2 to Sta. 6.

A marked seasonal cycle appears for $b_{bp}(555)$ at BOUSSOLE (Fig. 4A), with minimum values of $\sim 2 \times 10^{-4} \text{ m}^{-1}$ during January–February 2006, values between $\sim 5 \times 10^{-4}$ and $1 \times 10^{-3} \text{ m}^{-1}$ in summer and fall each year, and the largest values during spring phytoplankton blooms, at $\sim 4\text{--}5 \times 10^{-3} \text{ m}^{-1}$. The minimal values reported here for $b_{bp}(555)$ are close to the noise level of the instruments (which is $\sim 1 \times 10^{-4} \text{ m}^{-1}$; see Methods). A high day-to-day variability is superimposed onto this seasonal cycle. The total range of variation in b_{bp} is of ~ 1.5 orders of magnitude, which is less than the range of variation of $[Chl]$, with nearly two orders of magnitude ($[Chl]$ from 0.05 to 3–5 mg m^{-3}). The $[Chl]$ and b_{bp} cycles are in phase, with relative b_{bp} changes generally following those of chlorophyll, except in specific and very short-term events (e.g., the onset of the spring bloom in 2006) and more importantly during the winter of 2006–2007. In this latter case, $b_{bp}(555)$ is only slightly larger than in January–February 2006, whereas $[Chl]$ is five to 10 times larger. In addition, and unlike the rest of the time series, $b_{bp}(555)$ is inversely related to $[Chl]$ during this time. The b_{bp} spectral dependency, γ , varies from ~ 0.5 to 1 during the peak of the spring phytoplankton blooms to $\gamma \sim 3\text{--}4$ in summer and

fall. Overall, the seasonal pattern for γ is the opposite of that for $[Chl]$ and $b_{bp}(555)$.

In the SBC (Fig. 4B), the seasonality in $b_{bp}(555)$ is weaker than at BOUSSOLE, with only a factor of five between the highest values, at $\sim 0.01 \text{ m}^{-1}$ in May–June, and the minimum values, at $\sim 0.002 \text{ m}^{-1}$, found during the late fall and winter. These low values are close to the maximum reached at BOUSSOLE, illustrating the complementary nature of the two data sets (see the shaded area in Fig. 4A). The spectral dependency also roughly follows an inverted pattern as compared to $b_{bp}(555)$, with values of γ between about 0 and 2.

The b_{bp} vs. $[Chl]$ relationship—The data shown in Fig. 4A and B for $\lambda = 555 \text{ nm}$ and the data collected in the blue (442 nm) can be used to examine the relationship between $b_{bp}(442)$ or $b_{bp}(555)$ and chlorophyll. These findings are displayed in Fig. 5A (442 nm) and Fig. 5B (555 nm), along with the best-fit curve (solid line; linear regression on log-transformed data), the curves corresponding to the Morel and Maritorena (2001) semi-analytical model and the Huot et al. (2008) and Stramska et al. (2003) experimental results (respectively dotted, dashed, and dotted–dashed lines). The bilinear relationship of Behrenfeld et al. (2005), obtained at 440 nm from satellite-derived b_{bp} and $[Chl]$ values, is also displayed in Fig. 5A. These plots cover two orders of magnitude in b_{bp} values (2×10^{-4} to $2 \times 10^{-2} \text{ m}^{-1}$), which encompasses virtually the entire oceanic domain. The relationships that

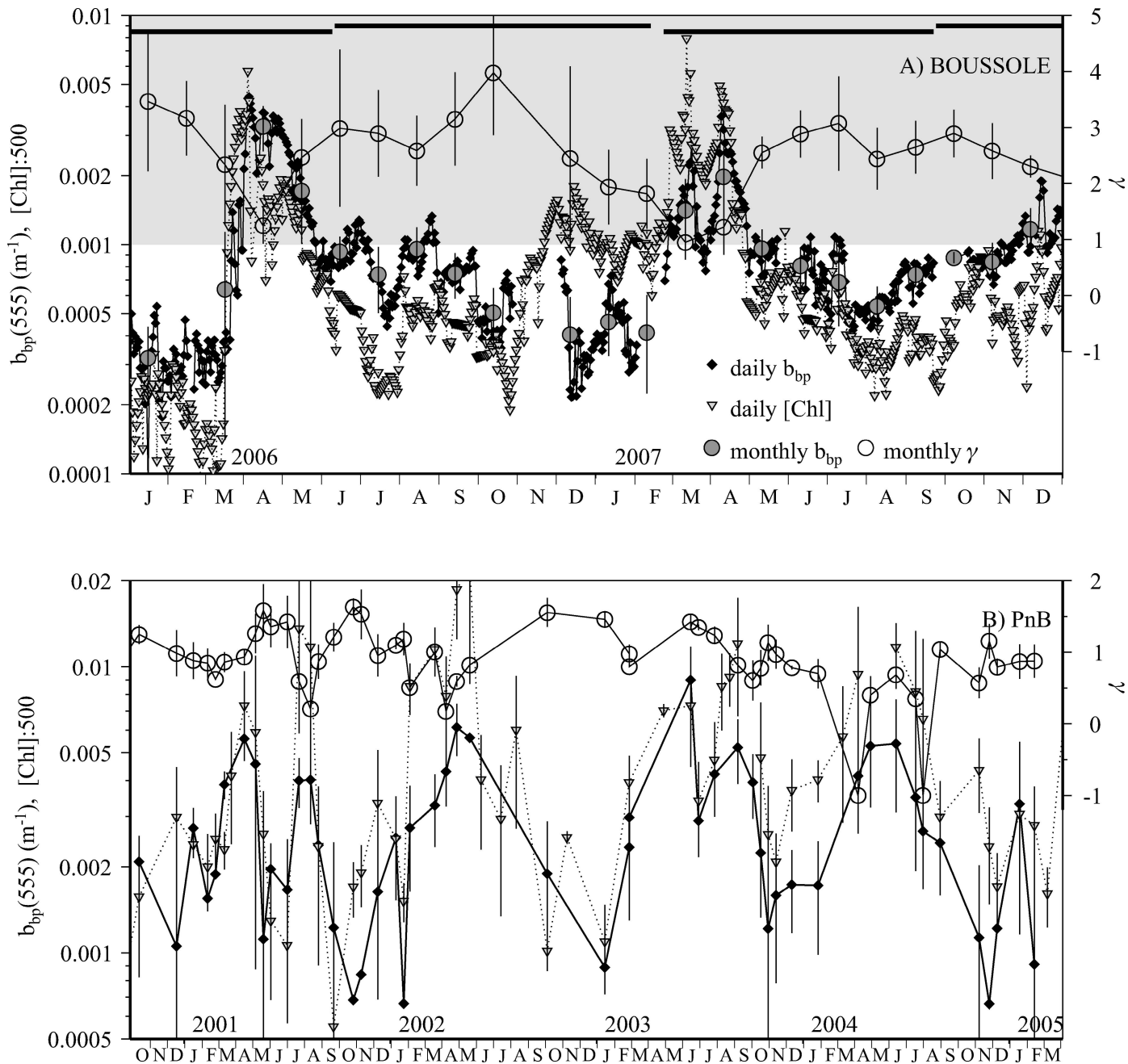


Fig. 4. (A) Time series at BOUSSOLE of $b_{bp}(555)$, $[Chl]$ (divided by 500 to match the b_{bp} scale), and γ . The $[Chl]$ shown here is the reconstructed cycle (see text and Antoine et al. 2008a). The horizontal bars on top of the figure show the duration of deployment for the different instruments (backscattering meters) used to build the time series. The shaded area corresponds to the range of variation for $b_{bp}(555)$ at PnB, as shown in (B). (B) Same as in (A), but for the average data over PnB Sta. 2–6. Note that here $b_{bp}(555)$ (not measured at PnB) is obtained by multiplying $b_{bp}(589)$ (measured at PnB) by the ratio (555:589) (i.e., assuming a λ^{-1} spectral dependency).

emerge are not significantly different from previous ones (regression statistics on the log-transformed data are reported on top of each panel). They do show a continuous decrease of b_{bp} with $[Chl]$, down to values of about $2 \times 10^{-4} m^{-1}$ in the green and $3\text{--}4 \times 10^{-4} m^{-1}$ in the blue (see also Huot et al. 2008). However, the average dispersion around the best-fit curve is large ($r^2 = 0.65$ at 442 nm and 0.74 at 555 nm). In addition, one data cluster is clearly out

of the average dispersion, centered on $[Chl]$ of $\sim 0.5 mg m^{-3}$ and $b_{bp}(442)$ of $\sim 0.0005 m^{-1}$ (arrow in Fig. 5A). These observations correspond to the period December 2006–January 2007 in the BOUSSOLE time series. The BOUSSOLE data dispersion is actually formed by several well-identified clusters of points corresponding to different periods of the year (e.g., winter mixing, phytoplankton bloom). It should be noted that the bilinear b_{bp} – Chl

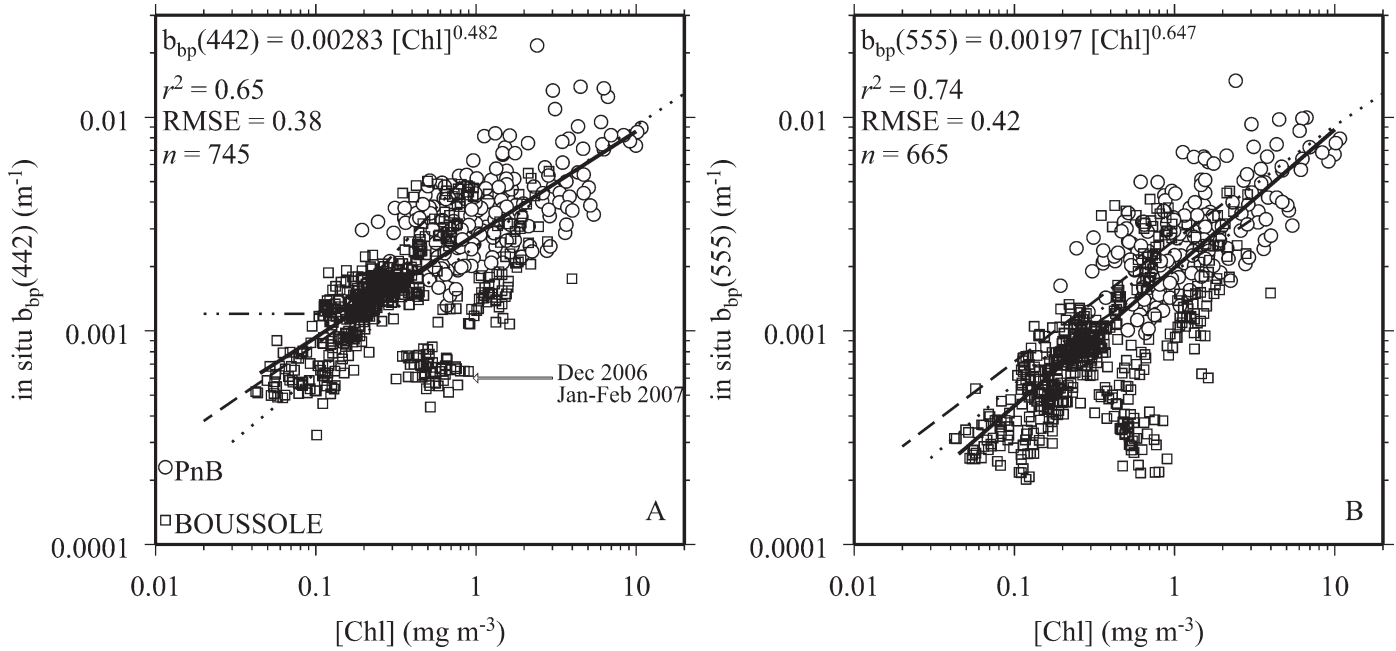


Fig. 5. Field determinations of b_{bp} as a function of $[Chl]$ for BOUSSOLE and PnB. (A) $\lambda = 442$ nm. (B) $\lambda = 555$ nm. The number of points and the parameters of a linear fit (thick solid line) on the log-transformed data are indicated on each panel. (A) The dashed line is the Huot et al. (2008) relationship, the dotted line is from the Morel and Maritorena (2001) model, and the dotted-dashed line is from fig. 1 in Behrenfeld et al. (2005). (B) The dotted line is as in (A), and the dashed line is from Stramska et al. (2003; their eq. 12).

relationship found in satellite inversion analyses (Behrenfeld et al. 2005; Siegel et al. 2005) is not observed with these two data sets. These issues will be discussed below.

The b_{bp} vs. c_p relationship—The b_{bp} vs. c_p relationships (Fig. 6A,B) are tighter than the b_{bp} vs. $[Chl]$ relationships.

Exponents of power-law fits are close to one for both 442 and 555 nm, indicating that changes in b_{bp} are nearly in proportion with changes of the particle load. This indicates that the particle nature (composition and PSD) only secondarily affects the relationship between b_{bp} and c_p for these two sites. The outlier data cluster identified for the

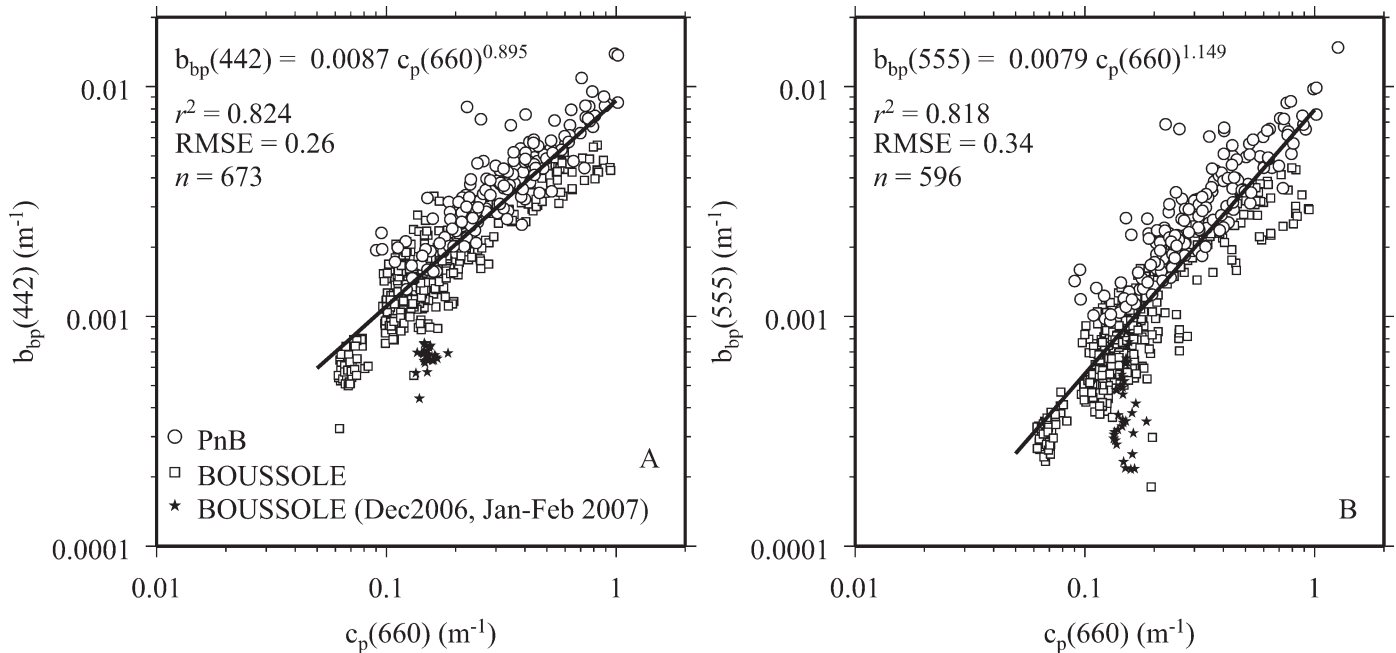


Fig. 6. Field determinations of b_{bp} as a function of the particulate beam attenuation coefficient at 660 nm, $c_p(660)$, for BOUSSOLE and PnB. (A) $\lambda = 442$ nm. (B) $\lambda = 555$ nm. The number of points and the parameters of a linear fit on the log-transformed data (thick solid line) are indicated on each panel.

period December 2006 to February 2007 in the b_{bp} vs. [Chl] relationships (Fig. 5) appears in Fig. 6, yet it is closer to being within the RMSE of the b_{bp} vs. c_p relationship. Another set of points appears separately from the overall data set in Fig. 6, although with low c_p values of ~ 0.06 – 0.07 m^{-1} . These data are for January and February of 2006, which were characterized by an exceptional vertical mixing of the water column with a mixed layer deeper than 2000 m (J.-C. Marty and J. Chiaverini pers. comm.), [Chl] of $\sim 0.05 \text{ mg m}^{-3}$, and a very low particle load. This situation actually persisted until mid-March, when phytoplankton bloomed so that c_p suddenly increased to values of $\sim 0.5 \text{ m}^{-1}$ within 2 d: hence, the jump on Fig. 6 between the lowest c_p and the rest of the data set (nearly no intermediate conditions). This ensemble of points is not, however, atypical of the general b_{bp} vs. c_p relationship.

The backscattering ratio—The time series of \tilde{b}_{bp} at $\lambda = 442$ and 555 nm are displayed in Fig. 7A for BOUSSOLE and Fig. 7B for PnB. Neither time series shows a clear seasonal cycle in \tilde{b}_{bp} . Average values at BOUSSOLE are 0.54% (standard deviation [SD] = 0.16) for $\lambda = 555 \text{ nm}$ and 1.01% (SD = 0.28) for $\lambda = 443 \text{ nm}$. At PnB, the values are 0.88% (SD = 0.25) for $\lambda = 555 \text{ nm}$ and 1.14% (SD = 0.29) for $\lambda = 443 \text{ nm}$. The \tilde{b}_{bp} ratios do not show a trend with [Chl] (Fig. 8). The spectral difference in \tilde{b}_{bp} from the blue to the green is larger at BOUSSOLE than at PnB.

Spectral dependence of particle backscattering—The γ parameter determined based on the BOUSSOLE and PnB data is plotted as a function of [Chl] in Fig. 9A and as a function of $b_{bp}(555)$ in Fig. 9B. There is an overall decrease of γ with increasing [Chl], with values of up to 3–4 when [Chl] is ~ 0.05 – 0.1 mg m^{-3} and values between 0 and 1 for larger concentrations. The slope of the best fit to the data is larger than that of other existing relationships (Morel and Maritorena 2001; Stramska et al. 2003; Huot et al. 2008) and closer to that of Loisel et al. (2006) (their fig. 7A), which was obtained from an inversion model using remotely sensed reflectances (Loisel and Stramski 2000). The γ parameter also exhibits significant correlation with $b_{bp}(555)$ (Fig. 9B; statistics on the figure). The dispersion is large, yet the upper envelope of the data set follows quite well the relationships obtained by Stramska et al. (2006) with data from the north polar Atlantic. These comparisons must be interpreted cautiously because of the different ways in which values of γ are determined by different investigations.

Discussion

Chlorophyll as an index or predictor of b_{bp} —The data displayed in Fig. 5 indicate a general relationship between b_{bp} and [Chl] in open ocean waters spanning 2.5 orders of magnitude in [Chl]. The least-square fits obtained here are consistent with previously published relationships also obtained from field measurements in the north polar Atlantic (Stramska et al. 2003), the south Pacific gyre (Huot et al. 2008), or the equatorial Pacific (Dall’Olmo et al. 2009). The scatter around the average fit here and in the

above previous studies is large; thus, aside from the first-order relationship, [Chl] is clearly not a great predictor of b_{bp} . Data in Fig. 5 essentially indicate that the average b_{bp} is higher when the average [Chl] is higher, with a large SD and significant outliers. In the [Chl] range of 0.3 – 2 mg m^{-3} there is virtually no relationship between b_{bp} and [Chl], while b_{bp} values span an order of magnitude for [Chl] $\sim 0.5 \text{ mg m}^{-3}$. Data plotted in Fig. 5 also show that the same low level of backscattering ($\sim 0.0005 \text{ m}^{-1}$ at 443 nm and 0.0002 m^{-1} at 555 nm) is exhibited by waters with an order of magnitude difference in their chlorophyll contents, from ~ 0.05 to $\sim 0.5 \text{ mg m}^{-3}$.

These results confirm the poor predictability of b_{bp} using [Chl] over a wide range of conditions, which is not entirely unexpected, as there are many cellular- and population-level processes that can affect the relationship between b_{bp} and [Chl]. Although phytoplankton cells themselves are not thought to be major contributors to b_{bp} (Stramski and Kiefer 1991; but see Dall’Olmo et al. 2009), recent work has indicated that photoadaptation and other physiological changes can alter the phytoplankton carbon (C) to Chl ratio (C : Chl) and likely the b_{bp} :Chl ratio (Behrenfeld et al. 2005). Furthermore, different phytoplankton groups and community structure will have different PSD, cellular geometries, and/or composition, all of which can lead to different b_{bp} –Chl relationships. Observations on phytoplankton cultures also show highly variable and species-dependent Chl– b_{bp} relationships (Whitmire et al. 2010).

The b_{bp} –Chl distribution from BOUSSOLE is further examined in Fig. 10 for $\lambda = 555 \text{ nm}$, with an expanded scale in order to magnify the differences between clusters of points. These clusters are identified by specific symbols (as indicated in the figure). The observations can be partitioned into two regimes, as symbolized by the two dotted lines in Fig. 10. From a [Chl] of ~ 0.3 to 1 mg m^{-3} , two distinct relationships appear, with a difference in b_{bp} by a factor of about 4 to 5 for a given [Chl]. After the intense winter mixing in January–February 2006 (circles in Fig. 10), a spring phytoplankton bloom abruptly developed, and [Chl] increased much faster than b_{bp} , which only increased from $\sim 0.0005 \text{ m}^{-1}$ to 0.001 m^{-1} when [Chl] went from ~ 0.05 to $\sim 1 \text{ mg m}^{-3}$ (black inverted triangles). Then b_{bp} increased by a factor of 5, while [Chl] only increased by a factor of 2. Assuming that changes in b_{bp} are a proxy for changes in phytoplankton biomass, this evolution indicates that the increase of the phytoplankton biomass came after a period of chlorophyll synthesis. This is actually detectable in Fig. 4, where the slope of the [Chl] curve around mid-March is steeper than that of the b_{bp} curve, before both parameters reach their maximum at the bloom peak (this corresponds to the top right-most points in Fig. 10). Immediately after the maximum of the bloom the points move to the second b_{bp} –Chl relationship, with nearly no transition between both because [Chl] rapidly drops while b_{bp} remains high (black inverted triangles to the left). This indicates a much lower phytoplankton growth and an increase in the detrital pool because of grazing and cell degradation. Then the points follow the second relationship during summer (diamonds and stars), with concomitant changes in b_{bp} and [Chl]. During this period, there is a

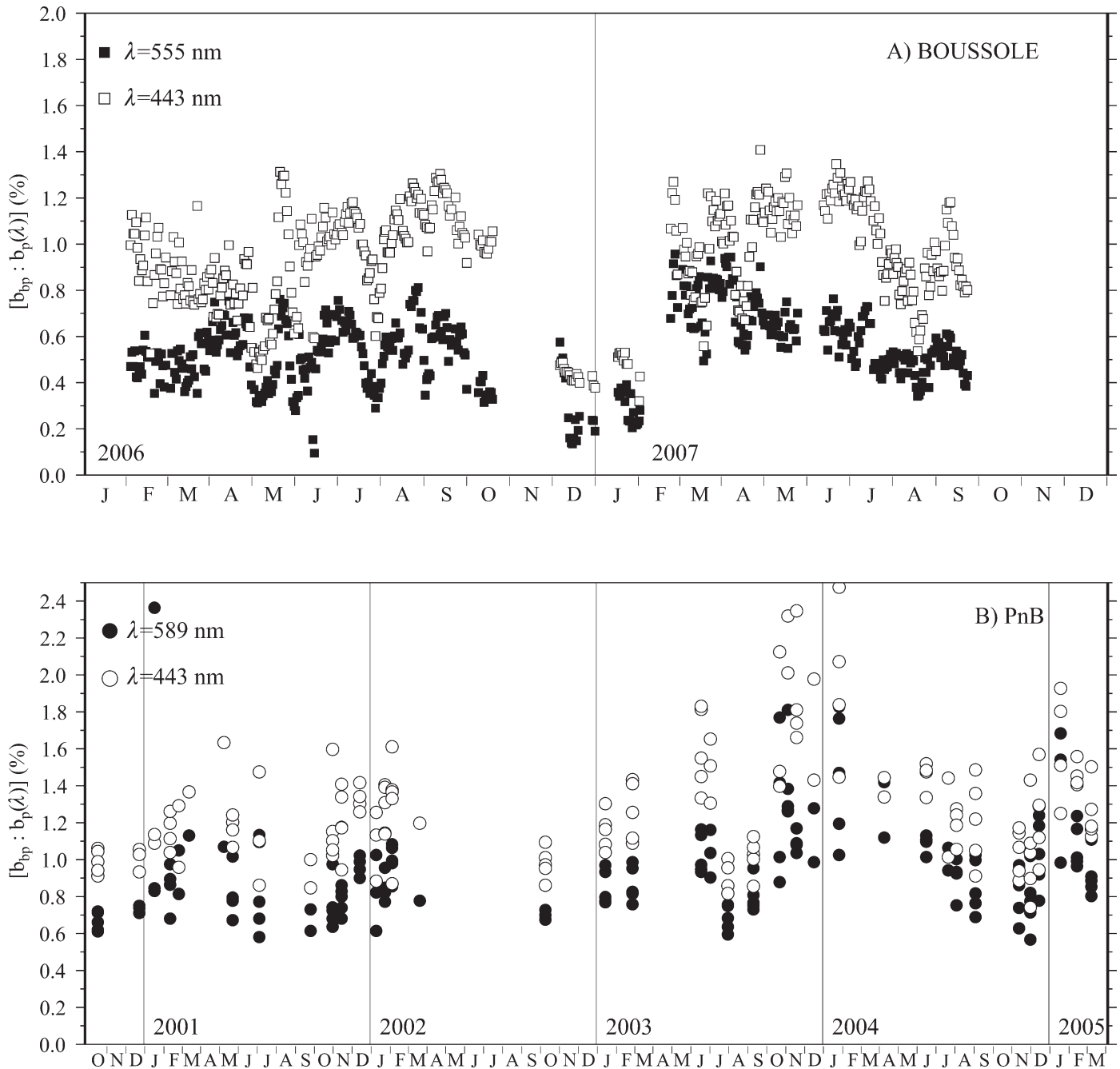


Fig. 7. Time series of the backscattering ratio at (A) BOUSSOLE and (B) PnB for $\lambda = 443$ and 555 nm, as indicated.

progressive removal of particles from the stratified upper layers (sinking and grazing). Finally, the points corresponding to the drop in b_{bp} observed in Fig. 4 at the end of March 2007 do not separately appear in Fig. 10, which indicates that this drop did not represent the decline of the phytoplankton bloom but rather a kind of dilution event.

The organization of the points in Fig. 10 as a set of well-identified clusters runs counter with the concept of a Case 1 ocean with continuously varying optical properties as a function of the chlorophyll concentration (Mobley et al. 2004). Instead, what is shown here indicates that bio-optical relationships might be described as a succession of

distinct regimes with rapid transitions among states. The same comment probably applies to spatial distributions as well (Dall'Olmo et al. 2009; Westberry et al. 2010). The 'continuum view' stems from forming global relationships by aggregating data collected around the World Ocean in varied environments. This continuum view does not hold well when examining a complete seasonal cycle at a given location at daily time resolution, as was done here. This leads one to question the sampling strategy that underlies decades of oceanographic cruises, which one could refer to as a 'pointillist approach' toward understanding the dynamics of ocean optical properties.

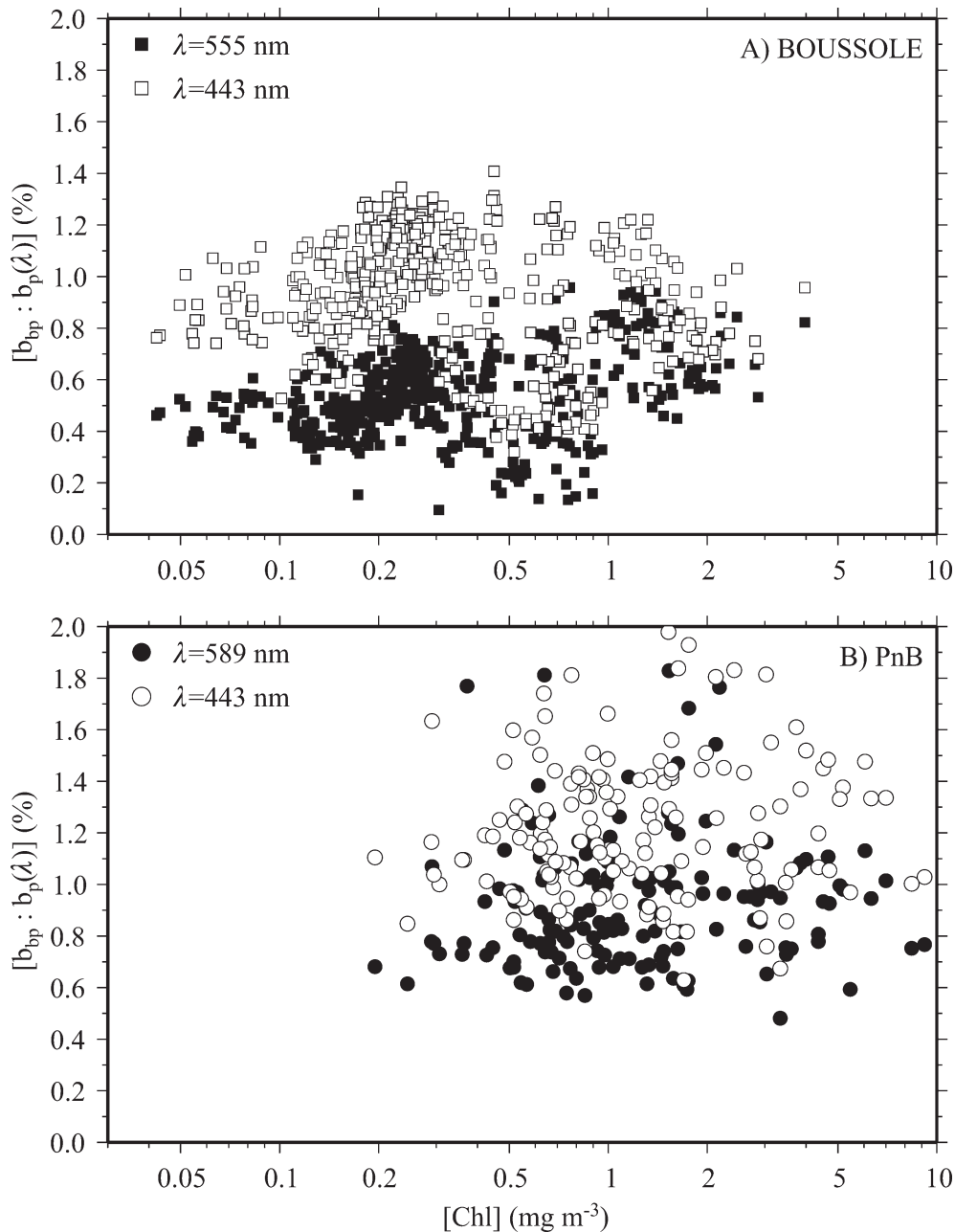


Fig. 8. Backscattering ratio as a function of [Chl] at (A) BOUSSOLE and (B) PnB and for $\lambda = 443$ and 555 nm (589 nm for PnB), as indicated.

Lessons learned from two contrasted winters at BOUSSOLE—The winter BOUSSOLE observations show the same low level of backscattering, while their chlorophyll contents differ by an order of magnitude (Figs. 5, 10). However, other data examined at BOUSSOLE changed in parallel to b_{bp} and [Chl]. These include the phytoplankton and particulate absorption coefficients, respectively a_p and a_p , whose ratio is informative related to the relative dominance of living phytoplankton within the particle pool, the c_p :Chl ratio (c_p^*), which gives an index of photoadaptation (as a proxy to the C:Chl ratio; phytoplankton adapted to higher light are expected to have higher C:Chl ratios), and the relative proportions of pico-,

nano- and micro-phytoplankton. The latter were determined from the HPLC-derived phytoplankton pigments, following the methods of Vidussi et al. (2001) and Uitz et al. (2006).

During the exceptional mixing event in January–February 2006, [Chl] was between ~ 0.05 and ~ 0.1 mg m^{-3} , c_p was ~ 0.03 m^{-1} , c_p^* was ~ 0.35 – 0.6 m^2 $(\text{mg Chl})^{-1}$, and the contribution of phytoplankton to the total particulate absorption ($a_p : a_p$) varied from $\sim 30\%$ to 75% (see Table 3). The relative contributions of pico- and micro-phytoplankton were stable and were both equal to $\sim 30\%$, so the relative contribution of nano-phytoplankton was $\sim 40\%$.

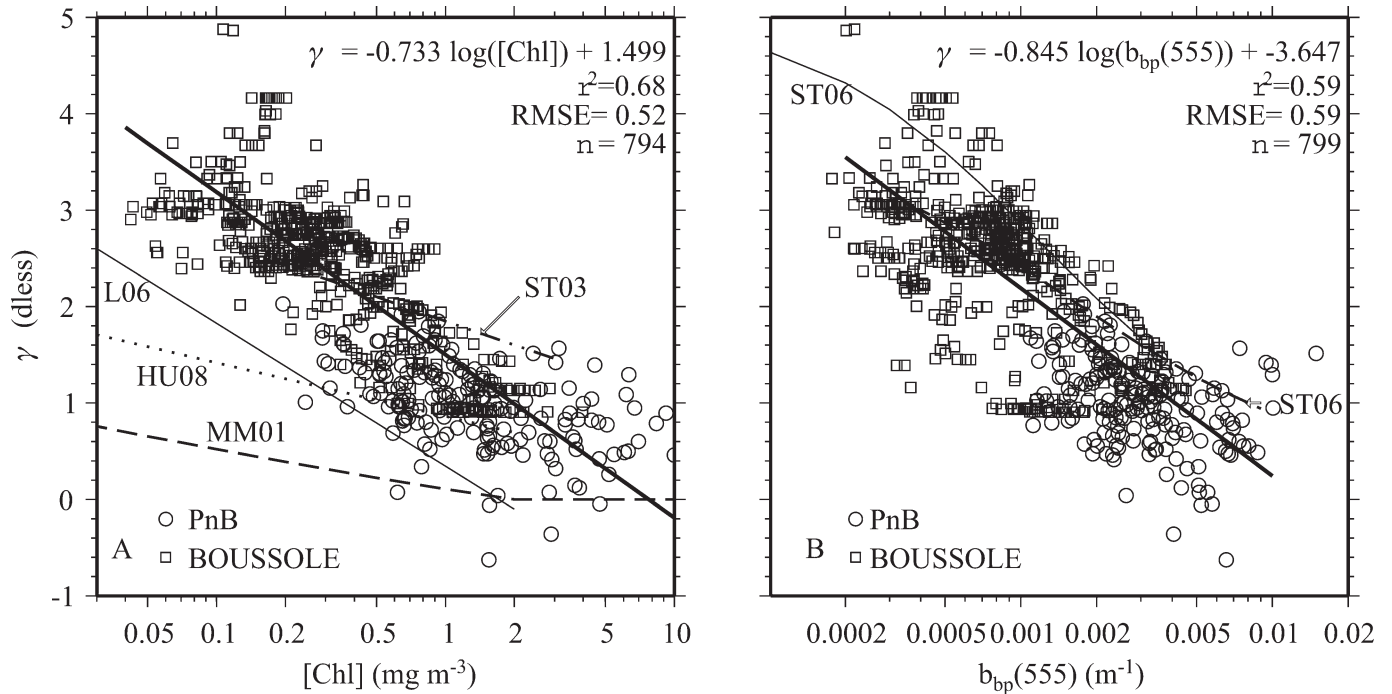


Fig. 9. Spectral dependency of b_{bp} (γ slope) as a function of (A) [Chl] or (B) $b_{bp}(555)$, for BOUSSOLE and PnB. (A) The number of points and the parameters of a linear fit (thick solid line) on the log-transformed data are indicated, where the dotted line is the Huot et al. (2008) relationship (noted HU08) the dashed line is from the Morel and Maritorena (2001) model (MM01), the dotted-dashed line is from eqs. 12 and 15 in Stramska et al. (2003) (ST03), and the thin solid line from fig. 7a in Loisel et al. (2006) (L06). (B) The continuous and dashed curves are the two relationships proposed by Stramska et al. (2006) (ST06; their fig. 11b) from data collected in the north polar Atlantic.

In the winter of 2006–2007, [Chl] was between ~ 0.5 and 1 mg m^{-3} , c_p was $\sim 0.1 \text{ m}^{-1}$, c_p^* was very low at $\sim 0.15 \text{ m}^2 (\text{mg Chl})^{-1}$, and the population of particles was dominated by phytoplankton ($a_\phi : a_p > 0.9$). The relative contribution of nano-phytoplankton was stable at 45%, and the relative contribution of pico-phytoplankton decreased from 45% to 35%, while that of micro-phytoplankton increased from 10% to 20% (from December 2006 to January 2007).

These data indicate that the situation in January–February 2006 (deep mixing), with low backscattering and very low particle load and chlorophyll concentrations, corresponds to a diluted population of particles essentially including detritus (low $a_\phi : a_p$ ratio) and in which phytoplankton were moderately photoadapted. This regime probably derives from the intense vertical mixing. On the contrary, the situation in December 2006–January 2007, with low backscattering and higher particle load and chlorophyll concentration, corresponds to a highly photoadapted phytoplankton population (adaptation to low light with very low c_p^*) with a minimal detrital contribution (high $a_\phi : a_p$ ratio).

The micro-phytoplankton contribution is considerably smaller (15%) during the winter of 2006–2007 as compared to the previous winter ($\sim 30\%$). Pico-phytoplankton, accordingly, increased. This change in the proportion of major size classes has no noticeable effect on the magnitude of b_{bp} . These small changes in b_{bp} may equally show that

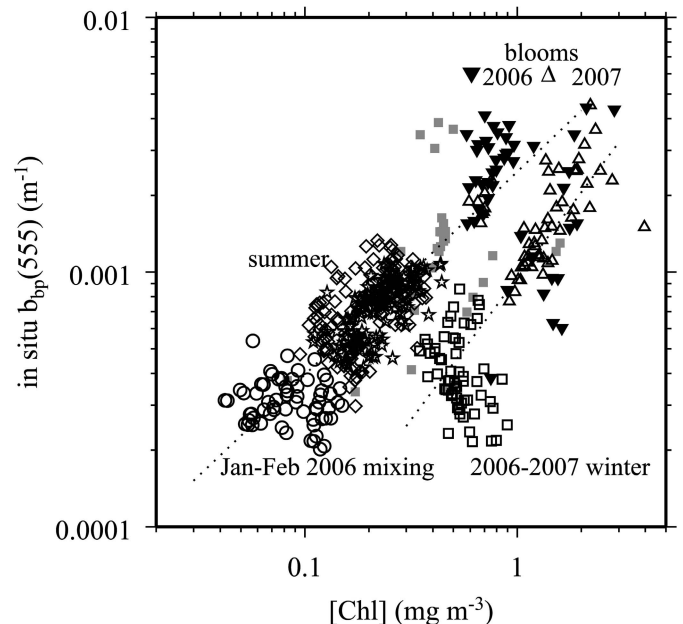


Fig. 10. $b_{bp}(555)$ as a function of [Chl] for BOUSSOLE only. Data are reproduced from Fig. 5A (see discussion for the meaning of symbols). Gray squares are data not falling into any of the categories identified on the figure. The two dashed lines are simply for illustration; they are not best-fit lines.

Table 3. Ecosystem bio-optical characteristics at BOUSSOLE during the two periods indicated.

Parameter	January–February	2006–2007
	2006 (intense mixing)	Winter
$b_{bp}(555)$ (m^{-1})	~0.0002–0.0005	
[Chl] ($mg\ Chl\ m^{-3}$)	0.05–0.1	0.5–1
c_p (m^{-1})	0.03	0.1
c_p^* [$m^2\ mg(Chl)^{-1}$]	0.35–0.6	0.15
$a_p : a_p$ (%)	30–75	>90
Picophytoplankton contribution (%)	30	45→35
Nanophytoplankton contribution (%)	40	45
Microphytoplankton contribution (%)	30	10→20

phytoplankton cells are not major contributors to backscattering (Morel and Ahn 1991; Ahn et al. 1992) or that physiological variability was compensated by abundance differences in determining b_{bp} . There is no obvious link between the change in γ (~ 3 in 2006 and ~ 2 in 2007) and the change in the relative proportions of the three phytoplankton size classes.

Therefore, minimal values of backscattering in oceanic waters likely correspond to very different bio-optical regimes, with either diluted assemblages of particles, including phytoplankton, with a low photosynthetic activity or more concentrated populations of particles dominated by large, healthy, and growing phytoplankton cells with high intracellular chlorophyll content. The first situation exhibits low backscattering simply because the concentration of all types of particles is low. The second situation may result from many intermingled effects that we cannot separately identify here. One hypothesis for this low backscattering would be that photoadapted phytoplankton cells are poor backscatterers, again supporting the notion that [Chl] is a poor predictor of b_{bp} (Ahn et al. 1992). This hypothesis is, however, contradicted in the case of heterogeneous layered cells (Kitchen and Zaneveld 1992; Zaneveld and Kitchen 1995).

Particulate beam attenuation and backscattering—Knowledge of the b_{bp} vs. c_p relationship in the open ocean is lacking because of the scarcity of concurrent measurements. The data assembled in Fig. 6 offer one of the most comprehensive views of this relationship (see also the recent work by Dall’Olmo et al. 2009 and Westberry et al. 2010). The correspondence of b_{bp} with c_p is tighter than with [Chl], with lower RMSE of the two power-law fits (Fig. 6). This is expected because both b_{bp} and c_p are likely better proxies of particle abundances than is [Chl]. It is unexpected, however, when assuming that b_{bp} and c_p are sensitive to different parts of the PSD (Morel and Ahn 1991; Stramski and Kiefer 1991) (i.e., b_{bp} being largely [although not exclusively] thought to be due to small particles and c_p to larger ones). These considerations derive from following the Mie theory for low refractive index

homogeneous spherical particles the size distribution of which obeys a power law. The correlation observed here between b_{bp} and c_p might indicate that the parts of the PSD that drive b_{bp} and c_p would have a larger overlap than previously thought or that they simultaneously change (Dall’Olmo et al. 2009; Westberry et al. 2010). Therefore, the relationship observed here between b_{bp} and c_p confirms the findings of Dall’Olmo et al. (2009), which further supports the possibility of deriving c_p from space (Stramska and Stramski 2005).

The $\tilde{b}_{bp}(\lambda)$ and its dependence on [Chl]—Knowledge of the $\tilde{b}_{bp}(\lambda)$ is even poorer than that of b_{bp} itself. One reason for this lack of information is the difficulty involved in experimentally determining its values from two quantities that both have their own uncertainties and with $b_{bp} \ll b_p$. The values obtained here at BOUSSOLE, from 0.2% to 1% (Figs. 7A, 8A), are rather at the low end of the expected range for b_{bp} in oceanic waters, in particular in the green (Morel and Maritorena 2001; Twardowski et al. 2007; Huot et al. 2008). The higher values at PnB, between $\sim 0.6\%$ and 2% , are typical of a more coastal environment (Petzold 1972). The specific feature of these two data sets is the absence of a decreasing trend with [Chl], which is predicted by most previously published relationships between \tilde{b}_{bp} and [Chl], although the correlations are often weak. These relationships were established either for shallow-water coastal environments (Sullivan et al. 2005), coastal to open ocean waters (Twardowski et al. 2001; Whitmire et al. 2007; Huot et al. 2008), or from a mix of field measurements and theory (Ulloa et al. 1994; Morel and Maritorena 2001). Therefore, when interpreting results from these relationships, it is difficult to deconvolve the intermingled roles of the variable [Chl] range and bio-optical regimes they considered, of the level of constraint they carried from the Mie theory, and the role of possibly large uncertainties in their determination of \tilde{b}_{bp} for low [Chl]. Rather, the observations shown here indicate no dependence of the backscattering ratio on [Chl] (Huot et al. 2008).

Some of the previously published relationships between \tilde{b}_{bp} and [Chl] have been derived from the ratio of a b_{bp} vs. [Chl] relationship to a b_p vs. [Chl] relationship (Huot et al. 2008), rather than through a fit to individual \tilde{b}_{bp} determinations. The compatibility between these approaches is examined here, by again displaying \tilde{b}_{bp} as a function of [Chl], for $\lambda = 443$ nm (Fig. 11A) and $\lambda = 555$ nm (Fig. 11B) for the BOUSSOLE data set. Three methods are used to determine \tilde{b}_{bp} , all of which use the same b_{bp} values determined from a b_{bp} vs. [Chl] relationship obtained similarly to the one shown in Fig. 5, but with only the BOUSSOLE data and differing based on the determination of b_p . The first technique (black squares in Fig. 11) used the b_p vs. [Chl] relationship determined from the BOUSSOLE AC-9 data (open circles and dashed line on Fig. 11). The two other techniques used existing b_p vs. [Chl] algorithms (i.e., Loisel and Morel [1998], gray squares, and Huot et al. [2008], open squares). Independent \tilde{b}_{bp} predictions from Morel and Maritorena (2001) and Huot et al. (2008) are also shown (dotted and continuous curves, respectively).

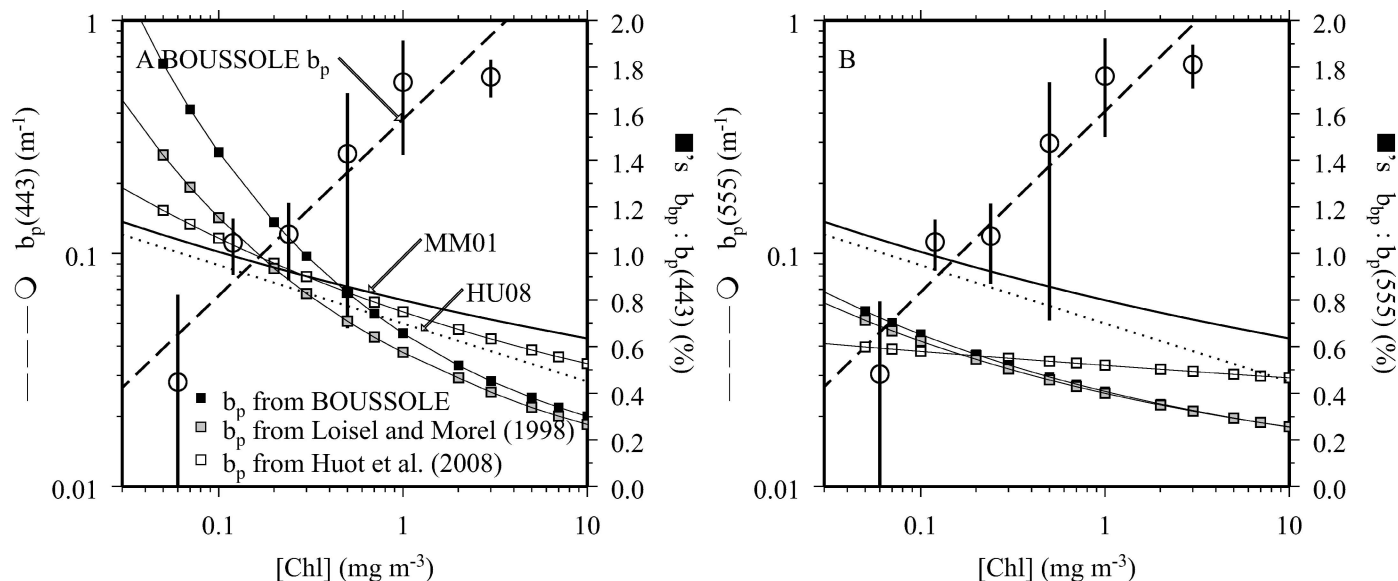


Fig. 11. (A) Particulate scattering coefficient at 443 nm, $b_p(443)$ (left scales) and particulate backscattering probability at the same wavelength, and $\tilde{b}_{bp}(443)$ (right scales) as a function of [Chl] for the BOUSSOLE data only. (B) Same as in (A) but for $\lambda = 555$ nm. The relationships of Morel and Maritorena (2001) and Huot et al. (2008) are indicated as MM01 and HU08, respectively.

Whatever the method used to determine b_p , dividing b_{bp} by b_p when both are obtained from their respective fits to [Chl] results in \tilde{b}_{bp} values that depend on [Chl]. For instance, $\tilde{b}_{bp}(443)$ (Fig. 11A) shows a decrease from ~ 1 – 1.5% to 0.3% when [Chl] increases from 0.03 to 10 mg m^{-3} . This decrease matches quite well the Morel and Maritorena (2001) model and the Huot et al. (2008) relationship when [Chl] $> \sim 0.2 \text{ mg m}^{-3}$. The \tilde{b}_{bp} values are higher than predicted by these models for low [Chl], however. The dependence on [Chl] (if any) is weak in the green (Fig. 11B), and the values are lower than the Morel and Maritorena (2001) or the Huot et al. (2008) predictions. These results show a Chl-dependent \tilde{b}_{bp} , which is inconsistent with the data displayed in Fig. 8 and discussed above. This disagreement indicates that deriving a \tilde{b}_{bp} vs. [Chl] relationship from the ratio of a b_{bp} vs. [Chl] relationship to a b_p vs. [Chl] relationship is invalid, probably because the coherence between individual and concomitant b_{bp} and b_p values is lost.

The \tilde{b}_{bp} ratio is dependent on the nature of particles and their size distribution (PSD). Although using Mie theory is questionable in terms of determining the \tilde{b}_{bp} magnitude and spectral dependence, it can be of some help in understanding relative changes in \tilde{b}_{bp} . The Mie-compliant Twardowski et al. (2001) model is accordingly used here to analyze the data clustering observed in Fig. 10. This model relates \tilde{b}_{bp} to the index of refraction of particles, n , and to the PSD slope (ζ), as derived from the spectral dependence of the particulate attenuation coefficient, c_p (Boss et al. 2001). The data are displayed in the \tilde{b}_{bp} – ζ space (Fig. 12A,C for BOUSSOLE and Fig. 12B,D for PnB). Symbols representing the various seasons at BOUSSOLE are as in Fig. 10. The BOUSSOLE data in Fig. 12A and C show (1) the lower PSD slopes (~ 2.5 to 3.3) during spring phytoplankton blooms, indicating an increased proportion of large particles; (2) no significant difference between the

two blooms, in spite of a dominance ($\sim 70\%$) of microphytoplankton in 2006 vs. nanophytoplankton in 2007 (not shown); (3) the largest PSD slopes during the deep vertical mixing in January–February 2006, confirming the dominance of small detrital particles in this regime; (4) still large slopes around 3.7 in summer 2006 and 2007; and (5) intermediate values associated with minimal refractive indices (~ 1.04) during the 2006–2007 winter. The average refractive indices are larger and the PSD slopes are lower at PnB (Fig. 12B,D), which is expected in such a coastal environment that is productive and may be influenced by minerogenic particle input (Kostadinov 2005). Changes in the refractive index dominate the \tilde{b}_{bp} changes at PnB, as compared to changes in the PSD. Identifying seasons in the PnB data would not reveal seasonal data clusters (not shown), as already observed from Fig. 4B.

Spectral dependency of the backscattering coefficient and the backscattering ratio—There is still much debate about the spectral dependency of scattering and backscattering by marine particles in oceanic waters. Semi-analytical models (Gordon et al. 1988; Morel and Maritorena 2001) rely on assumptions or considerations that derive from Mie theory and on some experimental evidence. Definitive answers have not been reached from field determinations, possibly because data were too few to provide confidence (Huot et al. 2008), with essentially unknown uncertainties (Whitmire et al. 2007), and were essentially coastal and cannot be applied to the global ocean (Loisel et al. 2007; Snyder et al. 2008).

The b_{bp} spectral dependency is quantified here through the γ parameter, which is determined by the composition, shapes, and size distribution of the particle assemblage. The intermingled contributions of these different parameters to changes in γ are still uncertain (Stramski et al. 2004). The combination of the BOUSSOLE and PnB data indicates a

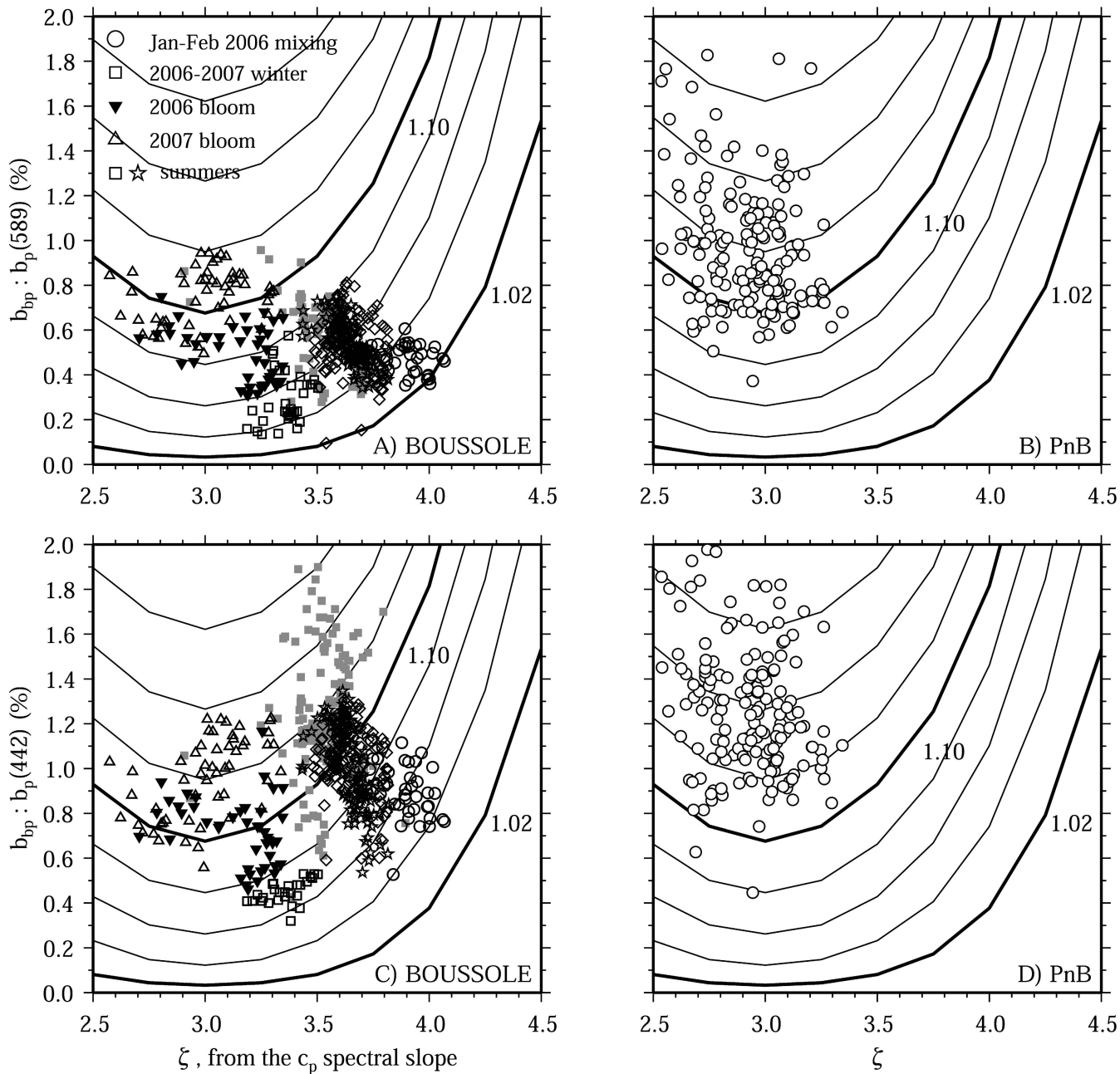


Fig. 12. \tilde{b}_{bp} plotted as a function of the PSD slope, ζ , at (A, B) $\lambda = 555$ nm and (C, D) $\lambda = 442$ nm at (A, C) BOUSSOLE and (B, D) PnB. The ζ slope is computed from the spectral dependence of c_p per eq. 6 in Boss et al. (2001) (and not from the b_{bp} spectral dependence shown in Fig. 9). The meaning of symbols for BOUSSOLE is as described in Fig. 10. The contour lines are from the model of Twardowski et al. (2001) for increasing values of the relative index of refraction n (increment is 0.02; thick curves are for $n = 1.02$ and 1.1).

significant spectral dependence for b_{bp} between the blue and the green when the chlorophyll concentration is low ($\gamma \sim 3$; i.e., a factor of ~ 2 from 555 to 443 nm; Fig. 9) and a weaker spectral dependence for larger chlorophyll concentrations (γ between 0 and 1). These b_{bp} spectral slopes are steeper than those in Morel and Maritorena (2001). They are, on average, closer to the spectral slopes derived by Huot et al. (2008) for [Chl] of > 0.3 mg m^{-3} and to those derived by Stramska et al. (2006) for [Chl] of < 1 mg m^{-3} . The overall change of γ with [Chl] found here is actually close to the one found by Loisel et al. (2006; their fig. 7A).

Gordon et al. (2009) also found a weak spectral dependence for total b_b (exponent between 0.4 and 1). The backscattering ratios displayed in Snyder et al. (2008) show a large range of significant spectral variations, yet their data are exclusively from turbid coastal waters. The wavelength range considered, the computation method, and the measurement uncertainties taken altogether influence the derived value of γ (McKee et al. 2009). The quantitative comparisons between investigators and instruments are therefore difficult, so the above comparison must be cautiously considered.

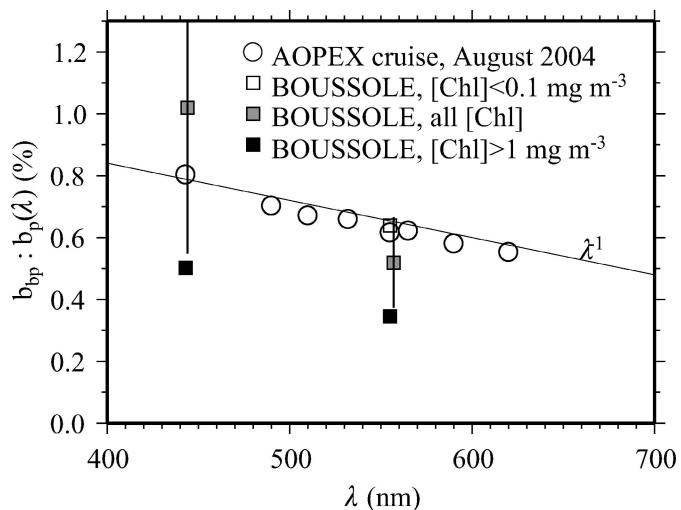


Fig. 13. \tilde{b}_{bp} as a function of wavelength for the data as indicated. Vertical lines are the SDs for the BOUSSOLE \tilde{b}_{bp} values computed for all [Chl]. The λ^{-1} spectral dependency is shown as a thin solid line.

When a spectral dependence is observed for b_{bp} , the question is whether it can be attributed to b_p or \tilde{b}_{bp} or to both. Again, when Mie theory is supposedly applicable to oceanic particles of low refractive index and distributed following a Jünger-type power law, \tilde{b}_{bp} should be spectrally neutral so the spectral effect is attributed to b_p (Ulloa et al. 1994; Morel and Maritorena 2001). When a weak spectral dependence is found, authors often prefer not to conclude in order not to violate theoretical assumptions (Whitmire et al. 2007). Huot et al. (2008) also concluded that \tilde{b}_{bp} was spectrally flat because they found a similar spectral dependence on b_{bp} and b_p over the spectral range of 412–660 nm. When looking more specifically at their data in the spectral range of 443–555 nm, however, b_p actually does not show any spectral dependence (their fig. 5), which would imply that \tilde{b}_{bp} does show such a dependence.

The b_p BOUSSOLE data (not shown) and the b_p PnB AC-9 data (see fig. 2 in Kostadinov et al. 2007) rather indicate that b_p is close to neutral, so the b_{bp} spectral dependence would essentially result from a spectral dependence of \tilde{b}_{bp} . The \tilde{b}_{bp} spectral values corresponding to the BOUSSOLE data shown in Fig. 7A are displayed in Fig. 13 (gray squares), along with values determined from the volume scattering function meter measurements on the BOUSSOLE site in August 2004 for an average [Chl] of 0.12 mg m^{-3} (open circles). The \tilde{b}_{bp} values are systematically larger in the blue than in the green, and the difference is more pronounced for low chlorophyll concentrations. The BOUSSOLE data used here show spectral slopes ranging from λ^{-1} for high [Chl] to λ^{-3} for low [Chl], which is quite high. The August 2004 MVSM data have a λ^{-1} slope. Low-[Chl] environments are expected to exhibit higher spectral slopes of b_{bp} (Loisel et al. 2006; Kostadinov et al. 2009), so if b_p is assumed to be relatively flat spectrally, these observations are consistent with a relative dominance of smaller particles (higher PSD slopes) in more oligotrophic environments.

Acknowledgments

We gratefully acknowledge David Menzies and Dave Court for help at sea and in data processing for the PnB project. For the BOUSSOLE project, Emilie Diamond and Grigor Obolensky provided help at sea and assistance with inherent optical properties data processing. Francis Louis was instrumental in the preparation and management of buoy deployments, and Joséphine Ras provided the quality of the HPLC data processing. BOUSSOLE is supported and funded by the Centre National de la Recherche Scientifique in terms of permanent staff and by the Institut National des Sciences de l'Univers in terms of ship time for the monthly cruises. Financial support is acknowledged from the Centre National d'Etudes Spatiales; the European Space Agency through European Space Research and Technology Center contract 14393/00/NL/DC and European Space Research institute contracts 17286/03/I-OL and 21770/08/I-OL; and the U.S. National Aeronautics and Space Administration (NASA; through a Letter of Agreement with the Université Pierre et Marie Curie). The captains and crews of the *Tethys-II R/V*, the *Castor-02* vessel (Foselev Marine company), and the *GG-IX* (IXsurvey and Samarov companies) are warmly thanked for their help at sea. PnB is supported by the NASA Ocean Biology and Biogeochemistry Program. Ship time for PnB is provided in collaboration with the U.S. National Oceanic and Atmospheric Administration Channel Islands National Marine Sanctuary. We also thank reviewers for their comments and suggestions, which helped improve the manuscript.

References

- AHN, Y. H., A. BRICAUD, AND A. MOREL. 1992. Light backscattering efficiency and related properties of some phytoplankters. *Deep-Sea Res. I* **39**: 1835–1855.
- ANTOINE, D., F. D'ORTENZIO, S. B. HOOKER, G. BÉCU, B. GENTILI, D. TAILLIEZ, AND A. J. SCOTT. 2008a. Assessment of uncertainty in the ocean reflectance determined by three satellite ocean color sensors (MERIS, SeaWiFS and MODIS-A) at an offshore site in the Mediterranean Sea (BOUSSOLE project). *J. Geophys. Res.* **113**: C07013, doi:10.1029/2007JC004472
- , P. GUEVEL, J.-F. DESTÉ, G. BÉCU, F. LOUIS, A. J. SCOTT, AND P. BARDEY. 2008b. The BOUSSOLE buoy—A new transparent-to-swell taut mooring dedicated to marine optics: Design, tests and performance at sea. *J. Atmos. Ocean Technol.* **25**: 968–989, doi:10.1175/2007JTECH0563.1
- , AND OTHERS. 2006. BOUSSOLE: A joint CNRS-INSU, ESA, CNES and NASA ocean color calibration and validation activity. National Aeronautics and Space Administration Technical Memorandum No. 2006-214147.
- BABIN, M., A. MOREL, V. FOURNIER-SICRE, F. FELL, AND D. STRAMSKI. 2003. Light scattering properties of marine particles in coastal and oceanic waters as related to the particle mass concentration. *Limnol. Oceanogr.* **48**: 843–859, doi:10.4319/lo.2003.48.2.0843
- BEHRENFELD, M. J., E. BOSS, D. A. SIEGEL, AND D. M. SHEA. 2005. Carbon-based ocean productivity and phytoplankton physiology from space. *Glob. Biogeochem. Cycles* **19**: GB1006, doi:10.1029/2004GB002299
- BISHOP, J. K. B. 1986. The correction and suspended mass calibration of Sea Tech transmissometer data. *Deep-Sea Res.* **33**: 121–134.
- BOHREN, C. F., AND S. B. SINGHAM. 1991. Backscattering by nonspherical particles—a review of methods and suggested new approaches. *J. Geophys. Res.* **96**: 5269–5277, doi:10.1029/90JD01138

- BOSC, E., A. BRICAUD, AND D. ANTOINE. 2004. Seasonal and interannual variability in algal biomass and primary production in the Mediterranean Sea, as derived from four years of SeaWiFS observations. *Glob. Biogeochem. Cycles* **18**: GB1005, doi:10.1029/2003GB002034
- BOSS, E., AND W. S. PEGAU. 2001. Relationship of light scattering at an angle in the backward direction to the backscattering coefficient. *Appl. Opt.* **40**: 5503–5507, doi:10.1364/AO.40.005503
- , M. LEE, M. S. TWARDOWSKI, E. SHYBANOV, G. KOROTAIEV, AND F. BARATANGE. 2004a. The particulate backscattering ratio at LEO-15 and its use to study particle composition and distribution. *J. Geophys. Res.* **109**: C01014, doi:10.1029/2002JC001514
- , D. STRAMSKI, T. BERGMANN, W. S. PEGAU, AND M. LEWIS. 2004b. Why should we measure the optical backscattering coefficient? *Oceanography* **17**: 44–49.
- , M. S. TWARDOWSKI, AND S. HERRING. 2001. Shape of the particulate beam attenuation spectrum and its inversion to obtain the shape of the particulate size distribution. *Appl. Opt.* **40**: 4885–4893, doi:10.1364/AO.40.004885
- BRICAUD, A., A. MOREL, AND L. PRIEUR. 1981. Absorption by dissolved organic matter of the sea (yellow substance) in the UV and visible domains. *Limnol. Oceanogr.* **26**: 43–53, doi:10.4319/lo.1981.26.1.0043
- , AND D. STRAMSKI. 1990. Spectral absorption coefficients of living phytoplankton and nonalgal biogenous matter: A comparison between the Peru upwelling area and the Sargasso Sea. *Limnol. Oceanogr.* **35**: 562–582, doi:10.4319/lo.1990.35.3.0562
- CHAMI, M., AND OTHERS. 2005. Optical properties of the particles in the Crimea coastal waters (Black Sea). *J. Geophys. Res.* **110**: C11020, doi:10.1029/2005JC003008
- DALL'OLMO, G., T. K. WESTBERRY, M. J. BEHRENFELD, E. BOSS, AND W. H. SLADE. 2009. Significant contribution of large particles to optical backscattering in the open ocean. *Biogeosciences* **6**: 947–967, doi:10.5194/bg-6-947-2009
- GORDON, H. R., O. B. BROWN, R. H. EVANS, J. W. BROWN, R. C. SMITH, K. S. BAKER, AND D. K. CLARK. 1988. A semianalytic radiance model of ocean color. *J. Geophys. Res.* **93**: 10909–10924, doi:10.1029/JD093iD09p10909
- , M. R. LEWIS, S. D. MCLEAN, M. S. TWARDOWSKI, S. A. FREEMAN, K. J. VOSS, AND G. C. BOYNTON. 2009. Spectra of particulate backscattering in natural waters. *Opt. Exp.* **17**: 16192–16208, doi:10.1364/OE.17.016192
- , AND A. MOREL. 1983. Remote assessment of ocean color for interpretation of satellite visible imagery: A review, p. 1–114. *In* R. Barber, C. Mooers, M. Bowman, and B. Zeitzschel [eds.], *Lecture notes on coastal and estuarine studies*. Springer Verlag.
- HARMS, S., AND C. D. WINANT. 1998. Characteristic patterns of the circulation in the Santa Barbara Channel. *J. Geophys. Res.* **103**: 3041–3065, doi:10.1029/97JC02393
- HUOT, Y., A. MOREL, M. S. TWARDOWSKI, D. STRAMSKI, AND R. A. REYNOLDS. 2008. Particle optical backscattering along a chlorophyll gradient in the upper layer of the eastern South Pacific Ocean. *Biogeosciences* **5**: 495–507, doi:10.5194/bg-5-495-2008
- KITCHEN, J. C., AND J. R. V. ZANEVELD. 1992. A three-layered sphere model of the optical properties of phytoplankton. *Limnol. Oceanogr.* **37**: 1680–1690, doi:10.4319/lo.1992.37.8.1680
- KOSTADINOV, T. S. 2005. Assessment of optical variability and closures in the Santa Barbara Channel, California using the Plumes and Blooms in situ dataset. M. A. thesis. Univ. of California, Santa Barbara.
- , D. A. SIEGEL, AND S. MARITORENA. 2009. Retrieval of the particle size distribution from satellite ocean color observations. *J. Geophys. Res.* **114**: C09015, doi:10.1029/2009JC005303
- , ———, AND ———. 2010. Global variability of phytoplankton functional types from space: Assessment via the particle size distribution. *Biogeosciences* **7**: 3239–3257, doi:10.5194/bg-7-3239-2010
- , ———, ———, AND N. GUILLOCHEAU. 2007. Ocean color observations and modeling for an optically complex site: Santa Barbara Channel, California, USA. *J. Geophys. Res.* **112**: C07011, doi:10.1029/2006JC003526
- LEE, M. E., AND M. R. LEWIS. 2003. A new method for the measurement of the optical volume scattering function in the upper ocean. *J. Atmos. Ocean Technol.* **20**: 563–571, doi:10.1175/1520-0426(2003)20<563:ANMFTM>2.0.CO;2
- LE QUÉRÉ, C., AND OTHERS. 2005. Ecosystem dynamics based on plankton functional types for global ocean biogeochemistry models. *Glob. Change Biol.* **11**: 2016–2040. doi:10.1111/j.1365-2486.2005.1004
- LOISEL, H., X. MÉRIAUX, J.-F. BERTHON, AND A. POTEAU. 2007. Investigation of the optical backscattering to scattering ratio of marine particles in relation to their biogeochemical composition in the eastern English Channel and southern North Sea. *Limnol. Oceanogr.* **52**: 739–752, doi:10.4319/lo.2007.52.2.0739
- , AND A. MOREL. 1998. Light scattering and chlorophyll concentration in Case 1 waters: A reexamination. *Limnol. Oceanogr.* **43**: 847–858, doi:10.4319/lo.1998.43.5.0847
- , J.-M. NICOLAS, A. SCIANDRA, D. STRAMSKI, AND A. POTEAU. 2006. Spectral dependency of optical backscattering by marine particles from satellite remote sensing of the global ocean. *J. Geophys. Res.* **111**: C09024, doi:10.1029/2005JC003367
- , AND D. STRAMSKI. 2000. Estimation of the inherent optical properties of natural waters from irradiance attenuation coefficient and reflectance in the presence of Raman scattering. *Appl. Opt.* **39**: 3001–3011, doi:10.1364/AO.39.003001
- MAFFIONE, R. A., AND D. R. DANA. 1997. Instruments and methods for measuring the backward-scattering coefficient of ocean waters. *Appl. Opt.* **36**: 6057–6067, doi:10.1364/AO.36.006057
- McKEE, D., M. CHAMI, I. BROWN, V. SANJUAN CALZADO, D. DOXARAN, AND A. CUNNINGHAM. 2009. Role of measurement uncertainties in observed variability in the spectral backscattering. *Appl. Opt.* **48**: 4663–4675, doi:10.1364/AO.48.004663
- MIE, G. 1908. Beiträge zur Optik trüber Medien, speziell kolloidaler Metallösungen, *Ann. Phys.* **330**: 377–445. [Contributions to optics of turbid media, in particular colloidal metallic solutions.], doi:10.1002/andp.19083300302
- MILLOT, C. 1999. Circulation in the western Mediterranean Sea. *J. Mar. Syst.* **20**: 423–442, doi:10.1016/S0924-7963(98)00078-5
- MOBLEY, C. D., D. STRAMSKI, W. P. BISSETT, AND E. BOSS. 2004. Optical modeling of ocean waters: Is the Case 1–Case 2 classification still useful? *Oceanography* **17**: 60–67.
- MOREL, A. 1973. Diffusion de la lumière par les eaux de mer. Résultats expérimentaux et approche théorique. North Atlantic Treaty Organization Advisory Group for Aerospace Research and Development lectures series No. 61, 3.1.1–3.1.76. [Light scattering in sea water. Experimental results and theoretical approach.]
- , AND Y.-H. AHN. 1991. Optics of heterotrophic nanoflagellates and ciliates: A tentative assessment of their scattering role in oceanic waters compared to those of bacterial and algal cells. *J. Mar. Res.* **49**: 177–202, doi:10.1357/002224091784968639

- , AND J.-M. ANDRÉ. 1991. Pigment distribution and primary production in the western Mediterranean as derived and modeled from coastal zone color scanner observations. *J. Geophys. Res.* **96**: 12685–12698, doi:10.1029/91JC00788
- , AND S. BÉLANGER. 2006. Improved detection of turbid waters from ocean color information. *Remote Sens. Environ.* **102**: 237–249, doi:10.1016/j.envres.2006.04.007
- , B. GENTILI, M. CHAMI, AND J. RAS. 2006. Bio-optical properties of high chlorophyll Case 1 waters and of yellow-substance dominated Case 2 waters. *Deep-Sea Res. I* **53**: 1439–1459, doi:10.1016/j.dsr.2006.07.007
- , AND S. MARITORENA. 2001. Bio-optical properties of oceanic waters: A reappraisal. *J. Geophys. Res.* **106**: 7163–7180, doi:10.1029/2000JC000319
- , AND L. PRIEUR. 1977. Analysis of variations in ocean color. *Limnol. Oceanogr.* **22**: 709–722, doi:10.4319/lo.1977.22.4.0709
- OTERO, M., AND D. A. SIEGEL. 2004. Spatial and temporal characteristics of sediment plumes and phytoplankton blooms in the Santa Barbara Channel. *Deep-Sea Res. II* **51**: 1129–1149.
- PETZOLD, T. J. 1972. Volume scattering functions for selected ocean waters. Scripps Institution of Oceanography, University of California, San Diego, SIO Reference 72-78, 10-01-1972.
- PREISENDORFER, R. W. 1961. Application of radiative transfer theory to light measurements in the sea. *Monogr. Int. Union Geod. Geophys. Paris* **10**: 11–30.
- RAS, J., J. UITZ, AND H. CLAUSTRÉ. 2008. Spatial variability of phytoplankton pigment distributions in the subtropical South Pacific Ocean: Comparison between in situ and modelled data. *Biogeosciences* **5**: 353–369, doi:10.5194/bg-5-353-2008
- SIEGEL, D. A., S. MARITORENA, N. B. NELSON, AND M. J. BEHRENFELD. 2005. Independence and interdependencies of global ocean color properties; Reassessing the bio-optical assumption. *J. Geophys. Res.* **110**: C07011, doi:10.1029/2004JC002527
- SNYDER, W. A., AND OTHERS. 2008. Optical scattering and backscattering by organic and inorganic particles in U.S. coastal waters. *Appl. Opt.* **47**: 666–677, doi:10.1364/AO.47.000666
- STRAMSKA, M., AND D. STRAMSKI. 2005. Variability of particulate organic carbon concentration in the north polar Atlantic based on ocean color observations with Sea-viewing Wide Field-of-view Sensor (SeaWiFS). *J. Geophys. Res.* **110**: C10018, doi:10.1029/2004JC002762
- , ———, R. HAPTER, S. KACZMAREK, AND J. STON. 2003. Bio-optical relationships and ocean color algorithms for the north polar region of the Atlantic. *J. Geophys. Res.* **108**: 3143, doi:10.1029/2001JC001195
- , ———, S. KACZMAREK, D. B. ALLISON, AND J. SCHWARZ. 2006. Seasonal and regional differentiation of bio-optical properties within the north polar Atlantic. *J. Geophys. Res.* **111**: C08003, doi:10.1029/2005JC003293
- STRAMSKI, D., E. BOSS, D. BOGUCKI, AND K. J. VOSS. 2004. The role of seawater constituents in light backscattering in the ocean. *Prog. Oceanogr.* **61**: 27–56, doi:10.1016/j.pcean.2004.07.001
- , AND D. A. KIEFER. 1991. Light scattering by microorganisms in the open ocean. *Prog. Oceanogr.* **28**: 343–383, doi:10.1016/0079-6611(91)90032-H
- SULLIVAN, J. M., M. S. TWARDOWSKI, P. L. DONAGHAY, AND S. A. FREEMAN. 2005. Use of optical scattering to discriminate particle types in coastal waters. *Appl. Opt.* **44**: 1667–1680, doi:10.1364/AO.44.001667
- TOOLE, D. A., AND D. A. SIEGEL. 2001. Modes and mechanisms of ocean color variability in the Santa Barbara Channel. *J. Geophys. Res.* **106**: 26985–27000, doi:10.1029/2000JC000371
- TWARDOWSKI, M. S., E. BOSS, J. B. MACDONALD, W. S. PEGAU, A. H. BARNARD, AND J. R. V. ZANEVELD. 2001. A model for estimating bulk refractive index from the optical backscattering ratio and the implications for understanding particle composition in Case I and Case II waters. *J. Geophys. Res.* **106**: 14129–14142, doi:10.1029/2000JC000404
- , H. CLAUSTRÉ, S. A. FREEMAN, D. STRAMSKI, AND Y. HUOT. 2007. Optical backscattering properties of the “clearest” natural waters. *Biogeosciences* **4**: 1041–1058, doi:10.5194/bg-4-1041-2007
- UITZ, J., H. CLAUSTRÉ, A. MOREL, AND S. B. HOOKER. 2006. Vertical distribution of phytoplankton communities in open ocean: An assessment based on surface chlorophyll. *J. Geophys. Res.* **111**: C0085, doi:10.1029/2005JC003207
- ULLOA, O., S. SATHYENDRANATH, AND T. PLATT. 1994. Effect of the particle size distribution on the backscattering ratio in seawater. *Appl. Opt.* **33**: 7070–7077, doi:10.1364/AO.33.007070
- VAN DE HULST, H. C. 1981. *Light scattering by small particles*. Dover.
- VIDUSSI, F., H. CLAUSTRÉ, B. MANCA, A. LUCHETTA, AND J.-C. MARTY. 2001. Phytoplankton pigment distribution in relation to the upper thermocline circulation in the Eastern Mediterranean Sea during winter. *J. Geophys. Res.* **106**: 19939–19956, doi:10.1029/1999JC000308
- WESTBERRY, T. K., G. DALL’OLMO, E. BOSS, M. J. BEHRENFELD, AND T. MOUTIN. 2010. Coherence of particulate beam attenuation and backscattering coefficients in diverse open ocean environments. *Opt. Express* **18**: 15419–15425, doi:10.1364/OE.18.015419
- WHITMIRE, A. L., E. BOSS, T. J. COWLES, AND W. S. PEGAU. 2007. Spectral variability of the particulate backscattering ratio. *Opt. Express* **15**: 7019–7031, doi:10.1364/OE.15.007019
- , W. S. PEGAU, L. KARP-BOSS, E. BOSS, AND T. J. COWLES. 2010. Spectral backscattering properties of marine phytoplankton cultures. *Opt. Express* **18**: 15073–15093, doi:10.1364/OE.18.015073
- ZANEVELD, J. R. V., AND J. C. KITCHEN. 1995. The variation in the inherent optical properties of phytoplankton near an absorption peak as determined by various models of cell structure. *J. Geophys. Res.* **100**: 13309–13320, doi:10.1029/95JC00451
- ZHANG, X., AND L. HU. 2009. Estimating scattering of pure water from density fluctuation of the refractive index. *Opt. Express* **17**: 1671–1678, doi:10.1364/OE.17.001671
- , ———, AND M.-X. HE. 2009. Scattering by pure water: Effect of salinity. *Opt. Express* **17**: 5698–5710, doi:10.1364/OE.17.005698

Associate editor: Dariusz Stramski

Received: 28 July 2010

Accepted: 13 January 2011

Amended: 16 February 2011